Meteoritics & Planetary Science 41, Nr 4, 607–631 (2006)
Abstract available online at http://meteoritics.org

The rate of small impacts on Earth

Philip A. BLAND[1, 2*] and Natalya A. ARTEMIEVA[3]

[1]Impacts and Astromaterials Research Centre (IARC), Department of Earth Science and Engineering, Imperial College London, South Kensington Campus, London SW7 2AZ, UK
[2]IARC, Department of Mineralogy, Natural History Museum, Cromwell Road, London SW7 5BD, UK
[3]Institute for Dynamics of Geospheres, Russian Academy of Sciences, Leninsky Prospect 38/6, Moscow, Russia 117939
*Corresponding author. E-mail: p.a.bland@imperial.ac.uk

(Received 8 July 2004; revision accepted 19 January 2006)

Abstract–Asteroids tens to hundreds of meters in diameter constitute the most immediate impact hazard to human populations, yet the rate at which they arrive at Earth's surface is poorly known. Astronomic observations are still incomplete in this size range; impactors are subjected to disruption in Earth's atmosphere, and unlike the Moon, small craters on Earth are rapidly eroded. In this paper, we first model the atmospheric behavior of iron and stony bodies over the mass range 1–10^{12} kg (size range 6 cm–1 km) taking into account deceleration, ablation, and fragmentation. Previous models in meteoritics deal with rather small masses (<10^5–10^6 kg) with the aim of interpreting registered fireballs in atmosphere, or with substantially larger objects without taking into account asteroid disruption to model cratering processes. A few earlier attempts to model terrestrial crater strewn fields did not take into account possible cascade fragmentation. We have performed large numbers of simulations in a wide mass range, using both the earlier "pancake" models and also the separated fragments model to develop a statistical picture of atmosphere-bolide interaction for both iron and stony impactors with initial diameters up to ~1 km. Second, using a compilation of data for the flux at the upper atmosphere, we have derived a cumulative size-frequency distribution (SFD) for upper atmosphere impactors. This curve is a close fit to virtually all of the upper atmosphere data over 16 orders of magnitude. Third, we have applied our model results to scale the upper atmosphere curve to a flux at the Earth's surface, elucidating the impact rate of objects <1 km diameter on Earth.

We find that iron meteorites >5×10^4 kg (2.5 m) arrive at the Earth's surface approximately once every 50 years. Iron bodies a few meters in diameter (10^5–10^6 kg), which form craters ~100 m in diameter, will strike the Earth's land area every 500 years. Larger bodies will form craters 0.5 km in diameter every 20,000 years, and craters 1 km in diameter will be formed on the Earth's land area every 50,000 years. Tunguska events (low-level atmospheric disruption of stony bolides >10^8 kg) may occur every 500 years. Bodies capable of producing hazardous tsunami (~200 m diameter projectiles) should strike the Earth's surface every ~100,000 years. This data also allows us to assess the completeness of the terrestrial crater record for a given area over a given time interval.

INTRODUCTION

The craters preserved on the lunar mare provide a record of the rate and size distribution of impactors over a mass range of ~10–10^{16} kg (20 cm–20 km diameter) for the last 3.3–3.7 Ga since the majority of mare basalts were emplaced (Hartmann et al. 1981; Heisinger et al. 2003). Constructing a similar curve for the number of impacts over a given mass at the surface of the Earth is complicated: the atmosphere disrupts many meteoroids (Melosh 1981), and craters are removed by erosion and tectonism, infilled, or simply go unrecognized. A combination of these factors has given rise to the long-recognized departure from the standard size-frequency distribution of near-Earth objects (NEOs) for terrestrial craters <10–20 km in diameter (Grieve and Shoemaker 1984). Figure 1 shows a compilation of relevant flux data for both the Earth's upper atmosphere and the Earth's surface, presented as the number of events over a given mass per year. Constructing a figure of this type involves a number of assumptions, as different studies express impactor flux in different ways. Some quote impactor mass, impactor energy, absolute magnitude, or resulting crater

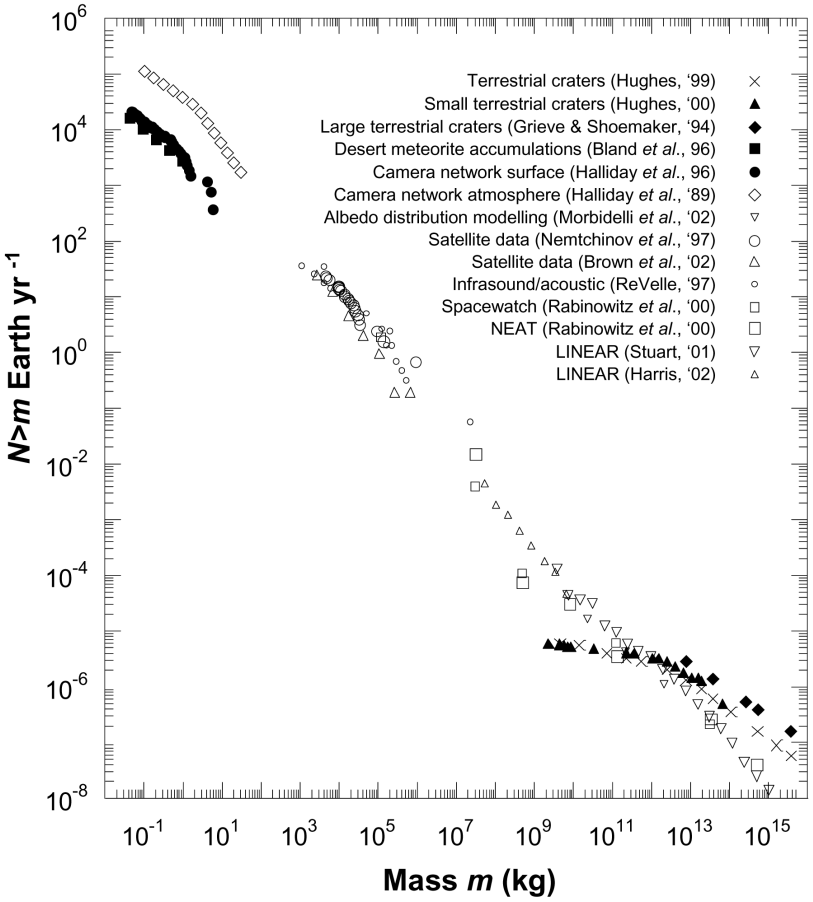

Fig. 1. A compilation of impact rate estimates for the upper atmosphere (open symbols) and the Earth's surface (closed symbols), presented as the number of events larger than a given mass for the whole Earth per year. Scaling flux estimates to impactor mass, rather than crater size, allows for both the upper atmosphere data and the non-crater producing meteorites to be shown on the same plot with larger bolides. The departure from the expected size-frequency distribution in the terrestrial crater data is evident in craters <10–20 km in diameter (5×10^{11}–7×10^{12} kg impactors), as is the paucity of data for the surface impactor flux in the 10^{1}–10^{11} kg region. Mass estimates are based on recovered mass (Bland et al. 1996); the authors' estimates of bolide mass derived from fireball data (Halliday et al. 1989, 1996; Nemtchinov et al. 1997); the authors' estimates of bolide diameter derived from fireball (Brown et al. 2002) or acoustic data (ReVelle 1997) or telescopic observations of NEOs (Rabinowitz et al. 2000; Morbidelli et al. 2002; Harris 2003), assuming an average density of 3000 kg/m^3 for impactors; scaling absolute magnitude of NEOs (Stuart 2001) after Rabinowitz et al. (2000); and scaling crater diameter (Grieve and Shoemaker 1994; Hughes 1999, 2000) to impactor mass after Schmidt and Housen (1987).

diameter, and so on. Scaling flux estimates to impactor mass, rather than crater size, conveniently allows all the upper atmosphere data, and also non-crater-producing meteorites, to be shown on the same plot with much larger crater-forming objects. Mass estimates are based on recovered mass in the case of meteorites (Bland et al. 1996); calculated estimates of bolide mass based on fireball data (Halliday et al. 1989, 1996; Nemtchinov et al. 1997); estimates of bolide diameter derived from fireball (Brown et al. 2002) or acoustic data (ReVelle 1997) or telescopic observations of NEOs (Rabinowitz et al. 2000; Morbidelli et al. 2002; Harris 2003), assuming an average density of 3000 kg/m^3 for meteoroids and NEOs; scaling absolute magnitude of NEOs (Stuart 2001) after Rabinowitz et al. (2000); and scaling crater diameter (Grieve and Shoemaker 1994; Hughes 1999, 2000) to impactor mass after Schmidt and Housen (1987), following the procedure of Ivanov (2001). Errors are specific to each study, and conversion to a single parameter involves assumptions that generate additional errors, but a number of broad trends are clear. The departure from the expected distribution in craters <10–20 km (5×10^{11}–7×10^{12} kg impactors) is evident, as is the lack of an independent constraint on surface impact rates in the 10^{1}–10^{11} kg region.

Since the terrestrial small crater record is incomplete, we have chosen to scale the known impactor flux at the upper atmosphere to a flux at the surface by modeling how a given bolide behaves in the atmosphere. The approach was outlined by Bland and Artemieva (2003). In this paper, we describe this method in more detail and review additional data that is relevant to estimating the impact rate both at the Earth's surface and the upper atmosphere.

Understanding the atmosphere-bolide interaction is

crucial to determining a flux for the surface, but accurately modeling the fragmentation and ablation behavior of bodies with different strength (from strong intact pieces to loose rubble piles), composition (from iron remnants of differentiated bodies to cometary snowballs), and mass (from cosmic dust to giant asteroids), is a nontrivial task. Although there were early attempts to model separated impactor fragments (Passey and Melosh 1980; Melosh 1989), most subsequent semianalytical approaches have simplified the problem by considering the impactor as a strengthless liquid-like object using so-called "pancake" models, in which clouds of fragments are modeled as a continuous deformed impactor (Melosh 1981; Chyba et al. 1993; Hills and Goda 1993; Hills and Goda 1998). In contrast, Artemieva and co-workers (Artemieva and Shuvalov 1996; Shuvalov et al. 2000; Artemieva and Shuvalov 2001) have developed a model that calculates motion, aerodynamic loading, and ablation for each individual particle or fragment. We have used the separated fragments (SF) model to understand fragmentation and ablation in the Earth's atmosphere for a range of impactor types and masses, in addition to a pancake model (Chyba et al. 1993), and a simple ablation model. The benefit of the SF model approximation is that it allows us to define a mass-velocity distribution on the surface for solid fragments that either create craters (in the case of high final velocity) or that may be found as meteorites (fragments with low final velocity). That is, for a given impactor at the top of the atmosphere, it allows us to predict the mass-velocity-size-distribution for that impactor at the surface. The results show a good agreement with the terrestrial meteorite and cratering record.

In addition, we obtain a size and frequency distribution for impactors at 1 AU over 16 orders of magnitude by fitting a compilation of flux data for the top of the Earth's atmosphere using a series of power laws. Knowledge of the fragmentation and ablation behavior for a given initial mass and impactor type allows us to estimate the energy and mass delivered to the surface so that the flux curve for the upper atmosphere can be scaled to an impact rate at the Earth's surface. A similar approach may be useful for Mars and Venus (Artemieva and Bland 2003).

NUMERICAL MODELING

Sophisticated hydrodynamic models are based on a full-scale two-dimensional or even three-dimensional hydrodynamic description of flow around an entering body. The meteoroid may be treated as a rigid nondeformable body, a strengthless liquid body (Crawford 1997; Shuvalov and Artemieva 2001), a swarm of noninteracting fragments (Svetsov et al. 1995), or as a solid body with internal strength (Ivanov et al. 1997). This kind of description is useful in modeling some particular events (such as the Tunguska event, or the Shoemaker-Levy 9 comet), but is not generally effective because physical constants defining the entry process (such as impact angle or pre-atmospheric velocity) or the projectile properties (such as ablation, strength, or shape) are poorly known, while limited computational time does not allow for the complete parameter space to be explored.

Equations to be Solved

For these reasons, simplified approaches that describe an entering projectile as a solid, nondeformable body are still widely used. In this case, the projectile motion in the atmosphere is described by a set of differential equations for drag, gravity, and ablation for the point mass (for example, Melosh 1989; Chyba et al. 1993):

$$\frac{dV}{dt} = -C_D\frac{\rho_g A V^2}{m} + g\sin\theta \tag{1}$$

$$\frac{dm}{dt} = -A\frac{\min(C_H\rho_g V^3/2, \sigma_{SB}T^4}{Q} \tag{2}$$

where V is the velocity, t = time, C_D and C_H = drag and heat transfer coefficients, ρ_g = atmospheric density, A = cross-sectional area of the body, m = its mass, g = gravity, Q = heat of ablation, σ_{SB} = Stephan-Boltzmann constant, T = temperature and θ = impact angle. The ablation coefficient, widely used in meteoritics, is defined as:

$$\sigma = \frac{C_H}{2C_D Q}$$

Combined with simple kinematical equations for:

entry angle, $\frac{d\theta}{dt} = \frac{g\cos\theta}{V}$

altitude, $\frac{dZ}{dt} = -V\sin\theta$

distance along trajectory, $\frac{dX}{dt} = V\cos\theta$

and atmosphere stratification, $\rho_g = \rho_g(Z)$

these equations result in reasonably accurate predictions for the trajectory of a meteoroid that travels through the atmosphere without breaking up.

However, fragmentation is a typical process for meteoroids larger than a few kg and leads to additional equations, which describe the spreading of a disrupted body in the pancake models of Chyba et al. (1993) and Hills and Goda (1993):

$$r\frac{d^2r}{dt^2} = C_D\frac{\rho_g V^2}{\rho_m} \tag{3}$$

(where r is the projectile radius) or, alternatively, repulsion of fragments in separated fragment (SF) models, caused by the interaction of bow shocks (Passey and Melosh 1980; Artemieva and Shuvalov 1996). In the latter case, the spreading velocity U for two identical fragments with density ρ_m, trajectory velocity V, disrupted at an altitude with atmospheric density g is defined as:

$$U = C_R V \sqrt{\frac{\rho_g}{\rho_m}} \quad (4)$$

with C_R = 0.01–1 from the analysis of the Earth's strewn fields (Passey and Melosh 1980). Melosh's idea is confirmed in 3-D modeling of disrupted meteoroid motion (Artemieva and Shuvalov 1996; Artemieva and Shuvalov 2001) and the coefficient of repulsion C_R for two identical fragments is defined as 0.45. If fragments have different masses, individual velocities are defined with conservation of momentum.

The pancake model, which allows a continuous description, is adequate for the so-called catastrophic fragmentation with a huge amount of fragments, while the SF model works better in the case of a few well-separated fragments. A hybrid model of "particles in the gas flow" is needed for intermediate scenarios (for discussion, see Artemieva and Shuvalov 2001).

Similar models are widely used in meteoritics to solve the inverse problem, i.e., to reconstruct meteorite properties on the basis of a meteoroid's trajectory, light, and acoustic effects (Ceplecha et al. 1993, Ceplecha and ReVelle 2005; Brown et al. 2002).

Here we combine the results of 3-D hydrodynamic modeling performed using the SOVA code (Shuvalov et al. 1999) for fragments' interaction (drag, ablation, and repulsion coefficients for different configurations of the fragments) (Artemieva and Shuvalov 1996, 2001) with differential equations for meteoroid motion. The model takes into account the deceleration (Equation 1), ablation (Equation 2), and successive fragmentation (Equation 4) of individual fragments. The meteoroid is subjected to disruption if dynamic loading exceeds tensile strength. Fragmentation of a single body results in two fragments with smaller mass and usually higher strength (although deviations from this rule are possible, with smaller fragments being weaker than larger ones), the same velocity along the trajectory, and an additional (usually substantially smaller than V) repulsion velocity U, perpendicular to the trajectory direction.

A random choice procedure is used to define the mass of the fragments and direction of repulsion in every disruption event. Each fragment is subjected to additional fragmentation later if the dynamic loading exceeds the updated fragment strength. Thus, the number of fragments changes in the process of the calculation from 1 (a parent body) to an arbitrarily large value, depending on the properties of the parent body and of the individual fragments (it is typically <10 for small iron bodies, and may exceed millions of fragments for a large weak projectile). While pancake models treat the disrupted meteoroid as a deformable continuous liquid, the SF approximation allows us to define a mass-velocity distribution on the surface for individual fragments that create craters (high final velocity) or occur as meteorites (fragments with low final velocity). The production of crater fields by small fragmented asteroids may therefore be simulated.

Input Parameters of the Model

A projectile strength depends on its type: stony meteoroids are usually weaker than stony-iron, which are weaker than iron meteoroids. The strength of individual fragments in compression and tension has been measured for a number of meteorites (or more accurately, their gram-size fragments). Tensile strength is usually in the range of 2×10^6 Pa to 6×10^7 Pa; compression an order of magnitude higher. There are few direct measurements of cometary strength, but most probably they are substantially weaker than asteroids (results from the Deep Impact experiment, avabilable online at http://deepimpact.jpl.nasa.gov, will provide valuable insight). However, the dynamic strength, which is derived from the dynamic pressure value at the moment of disruption in the atmosphere, may differ from the results of static experiments (Grady and Lipkin 1980), and rarely exceeds 5×10^6 Pa (Ceplecha et al. 1993). One possible explanation is that large bodies have pre-atmospheric internal "structure," i.e., faults and cracks. Gault et al. (1972) and Fujiware (1980) noted that the fracture strength of rock in static tests typically decreases as the size of the rock sample increases. Brittle fracture is due to the growth and coalescence of cracks. According to the classical Griffith model, cracks of length s begin to grow when they are subjected to a tensile stress above a critical value, which is proportional to $s^{-1/2}$. Therefore, large cracks are activated at lower stresses than small ones. Static fracture is controlled by the largest cracks because they activate at the lowest stresses. If the size of the largest crack in a rock sample is proportional to the sample size R, then the fracture strength should vary as $R^{-1/2}$. Large bodies are therefore weaker than small ones, and asteroids should fracture at much lower specific energies than individual meteorites. Farinella et al. (1982, 1983) arrived at similar conclusions for different reasons. Weibull statistics (1951) define the strength dependence of bodies with size: $\sigma_f = \sigma_0(m_0/m_f)^a$, where σ_0 and σ_f are strength of the body with mass m_0 and m_f, respectively; the α-coefficient depends on the projectile type and size (see Tsvetkov and Skripnik 1991 and Svetsov et al. 1995 for more details).

Two types of projectile are principally considered here: irons with a density of 7800 kg/m^3, strength of 4.4×10^8 dyn/cm^2 (for 1 kg sample, Zotkin and Tsvetkov 1983), and

ablation coefficient of 0.07 s^2/km^2 (in accordance with theoretical calculations by ReVelle and Rajan [1988], and with observations of U.S. Prairie Network fireballs identified as irons, ReVelle and Ceplecha [1994]); and stones with a density of 3400 kg/m^3 (mineral grain density of 3700 kg/m^3 and ~10% porosity) (Consolmagno et al. 1998), ablation coefficient of 0.014 s^2/km^2 (calculated for the Lost City fireball, and close to the average for stony bolides, see Ceplecha et al. 1993), and 10× lower strength than irons. The parameters for stones were chosen to define approximate upper limits on strength and density: larger stony bodies in the atmosphere and carbonaceous bolides may well have significantly lower strength and density.

All simulations were at asteroidal impact velocity of 18 km/s (this value is close to 17.95 km/s, estimated by Shoemaker [1977], and it is a reasonable compromise between 17.3 km/s from Ivanov et al. [2001] and 20.18 km/s from Rabinowitz [1993]), and an average entry angle of 45° (Gilbert 1893; Shoemaker 1962). The influence of varying impact angle was checked, and the average over all angles was found to be equal to a 45° impact.

Deriving a Statistical Average from a Stochastic Process

We performed 16 sets of SF model simulations for stony impactors and 16 sets for irons for bodies from 1 kg to 10^8 kg with a mass step of 0.5 log units (i.e., for 100 kg projectiles, 316 kg, 1000 kg, etc.). Each simulation was repeated 20–100 times to derive average data for each impact mass. For constant input parameters (drag, ablation, etc.) the results of each run may differ because of the random choice procedure used for fragments' mass definition. However, the final mass value is rather stable with average deviation over 20 runs being less than 10% (for a pre-atmospheric mass of 10^5 kg—deviation is larger than this for smaller masses, and smaller for large masses). An increase to 40–100 runs for a given mass does not change an average deviation substantially. At the same time, the mass of the largest fragment (and hence its velocity) varies significantly—sometimes by as much as a factor of two. Moreover, our experience with modeling the Sikhote-Alin iron shower (Artemieva and Shuvalov 1999) shows that additional variations of fragment strength are needed to reproduce the resulting strewn field, i.e., the average strength defined by Weibull statistics is valid only on average, while each fragment may have a unique individual strength. Thus, we use two sets of runs: The first with pure Weibull statistics, and the second with strength variations around an average value with different deviation values. The first set undoubtedly gives substantially more stable results for the total final mass (as discussed above) and usually fewer fragments than the second set. In the second set, variations of the final mass depend on the allowed deviation in strength, and this is higher than for the first set; the number of fragments is usually larger; mass and velocity of the largest fragment may differ significantly from run to run. It is easy to imagine that a very strong object can reach the surface without any fragmentation, i.e., only ablation would define its final mass, while a very weak object is subjected to continuous fragmentation, with no large fragments reaching the surface. Thus, our model with average Weibull statistics gives not an exact value, but a reasonable approximation. Every real impact event has its own unique properties and should not be described statistically, but rather individually. However, our model results provide an averaged statistical picture of atmosphere-bolide interaction over the 1–10^8 kg mass range for both iron and stony impactors. We use pancake model results (restricting lateral spreading to 2–4× initial radii) for bodies larger than 10^8 kg.

Restrictions of the Model

It is clear from observations and previous models that fragmentation is an important process for all incoming bodies larger than a few kg. We cannot define an upper limit for bolide fragmentation, although we can estimate it theoretically. The fragmentation (followed by separation) time is linked to crack growth. The speed of this process is $V_{cr} = 0.4C$, where C is the speed of sound in the material. Thus, fragmentation time is $t_{fr} = D/V_{cr}$, where D is the asteroid diameter. If this time is less than the travel time of the body within the atmosphere ($t_{fl} \sim 100/V$, where V is impact velocity), then fragmentation is not essential. Hence, for 10 km-size bodies $t_{fl} < t_{fr}$, and these objects strike the surface intact.

Another limitation of the SF model is a poor separation of the fragments, discussed in some detail in Artemieva and Shuvalov (1996). The model should be used with precautions for bodies with mass larger than 10^7–10^8 kg (larger than tens of meters in diameter). However, this does not mean that the pancake model gives better results in this mass range: the usage of the pancake model without restrictions on radius growth (Equation 3) leads to physically incorrect results. Detailed numerical modeling (O'Keefe et al. 1994; Shuvalov and Artemieva 2002) shows that hydrodynamic instabilities prevent the projectile from expanding to a diameter larger than 2–4× the initial diameter, in contrast with the original pancake model which predicted expansion to 20× the initial diameter.

RESULTS

SF and Pancake Model Output

The model results can be presented in a variety of ways. Below we show a few examples from particular runs, as well as averaged statistical data over all runs.

Impact Angle

The impact angle may influence crater size, crater field morphology, and the mass and final velocity of impacting

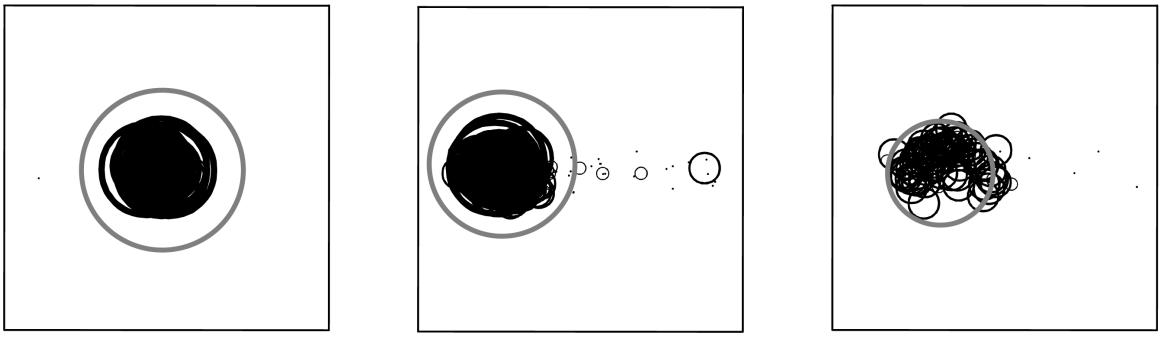

Fig. 2. Variation in the size and morphology of final craters (single craters formed by simultaneous impact of multiple fragments) with the impact angle. Crater fields formed from the impact of an iron projectile with an initial mass of 10^8 kg, with impact angles of 90°, 45°, and 30° (from left to right). Grey circles show estimates for the final crater (produced by joint fragments), with craters ~1 km, 0.9 km, and 0.5 km in diameter, respectively.

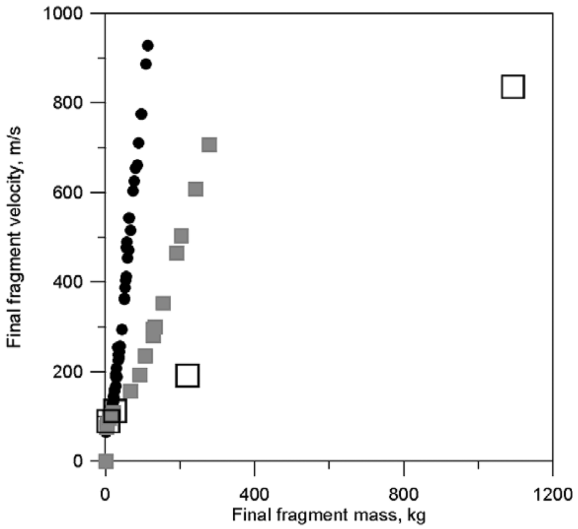

Fig. 3. The velocity of impacting fragments from a disrupted iron meteoroid versus mass for various impact angles. Initial (pre-atmospheric) mass is 2.5×10^4 kg. Impact angles are: 90° (vertical impact) = black circles, 45° = gray squares, and 30° = open squares. Shallower impact angles produce a smaller amount of large fragments. Total final mass decreases as impact angle decreases (2260 kg, 1820 kg, and 1340 kg, respectively).

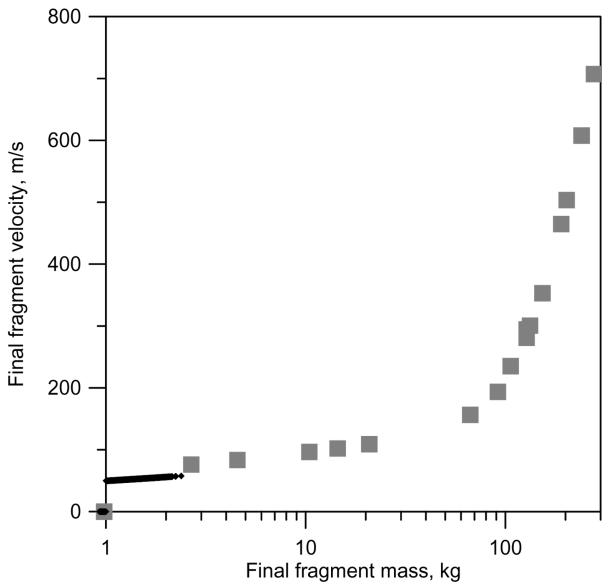

Fig. 4. Final masses and velocities for iron (gray squares) and stony (black dots) fragments. Initial conditions are identical: mass = 2.5×10^4 kg, velocity = 18 km/s, angle = 45°. Stony fragments are as a rule much smaller and have lower impact velocities. While the iron asteroid creates a cluster of craters, the stony body may only be found as meteorites.

fragments. Looking at small bodies, we see that the impact angle controls the velocity and final mass of impacting fragments. Figure 3 shows the velocities of final impacting fragments versus mass for a disrupted iron meteoroid with initial mass 2.5×10^4 kg. Comparing results for different impact angles, we see that shallow impact angles produce a smaller amount of larger fragments. Total final mass also decreases with impact angle, from 2260 kg (9% of the initial mass) at vertical impact to 1340 kg (5% of the initial mass). In larger bodies, the impact angle controls the morphology of resulting crater fields, and crater size. In Fig. 2, the results of iron body fragmentation in the atmosphere (projectile with initial mass 10^8 kg) are represented in the form of simulated crater strewn fields for various entry angles. We see a single simple crater of ~1 km in diameter in a 90° impact, and a 0.5 km diameter crater, and a developing crater field, in a 30° impact.

Fragment Size and Impact Velocity

Stony objects generally fragment much more, the fragments are much smaller, and these fragments have lower impact velocities. Figure 4 shows the difference in final velocity and fragmentation between iron and stone impactors with identical initial conditions. While the fragments of a disrupted iron object strike the surface with a velocity of 100–700 m/s and create multiple craters, pits, and meteorites (similar to Sikhote-Alin iron shower), the fragments of a

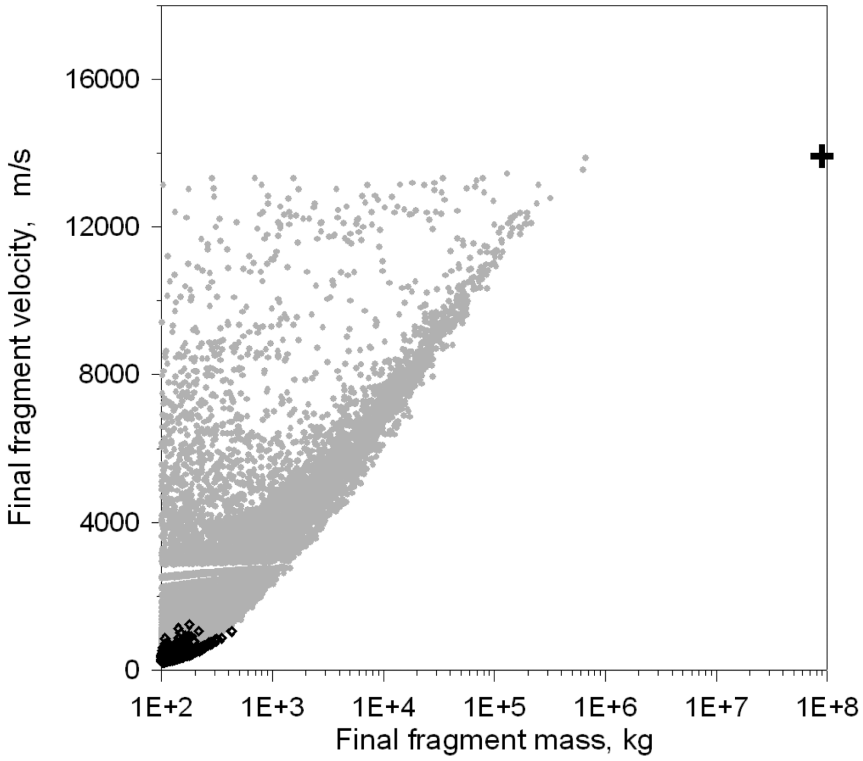

Fig. 5. Final fragment velocities versus final fragment mass for a pre-atmospheric iron body of 10^8 kg. Black diamonds illustrate a "regular" disruption, where the strength of the fragments depends only on their mass (a Weibull distribution). In this case, all fragments are rather small and have low terminal velocities with small variations. Grey circles show disruption with small variations in strength (dispersion = 0.02 from the average value, defined by the same law as in the first case). This can be thought of as more accurately approximating to the real nature of the impactors, while the Weibull law is correct on average. Variations in the final masses and velocities of fragments are now much higher. The black cross shows the result of a pancake model simulation with spreading to 2× initial radius.

stony body arrive at the surface with a velocity of less than 50 m/s and will only be found as meteorites. The final impact velocity of fragments begins to increase rapidly at masses >100 kg.

It is apparent that our choice of model has a substantial effect on estimates of final impact velocity. In Fig. 5, we again show final fragment velocity and fragment mass (for a 10^8 kg iron body), but present a comparison of model conditions: a "regular" disruption (black diamonds), where fragment strength depends only on mass (a Weibull distribution); a disruption with small variations in strength around a Weibull distribution, which perhaps more accurately approximates the real nature of impactors (grey circles); and the result of a pancake model simulation with spreading to 2× initial radius (black cross). A simple Weibull distribution predicts small fragments with low terminal velocities and little variation. Applying a small (~10%) variation in strength produces a substantial variation in final fragment mass and velocity, with fragment mass and velocity now much higher. In Fig. 6, we extend this analysis to look at the mass (top figure) and final velocity (middle figure) of the largest surviving fragment, and the resulting crater diameter (bottom), for various pre-atmospheric iron bodies. Note that this represents the crater diameter for each final fragment—not the combined total diameter of the crater made by multiple fragments. Four different model conditions are considered. The solid black line is shown for reference and applies to entry without fragmentation (a highly unlikely circumstance, producing a substantial overestimation in mass, velocity, and crater size). The solid gray line represents fragmentation as described by the pancake model. The dashed line shows regular fragmentation described by Weibull statistics and the dotted line Weibull statistics for strength with a 10% deviation from the average—plausibly the most realistic scenario. It is noteworthy that final velocities in many of these events may be significantly lower than generally assumed, a fact recently highlighted by Melosh and Collins (2005) (although these workers did use rather high-spreading radii in their pancake model). But as this discussion shows, it is clear that our choice of model has a significant effect on surviving mass, fragmentation, and impact velocity.

Impactor Mass and Energy

Figures 7 and 8 show a variety of SF model outputs. Mass and energy per unit area (area is constrained to that region within which 95% of the final mass falls) for a given pre-entry mass and projectile type are indicated in Figs. 7a and 7b. For larger masses (i.e., bodies larger than typical meteorites which

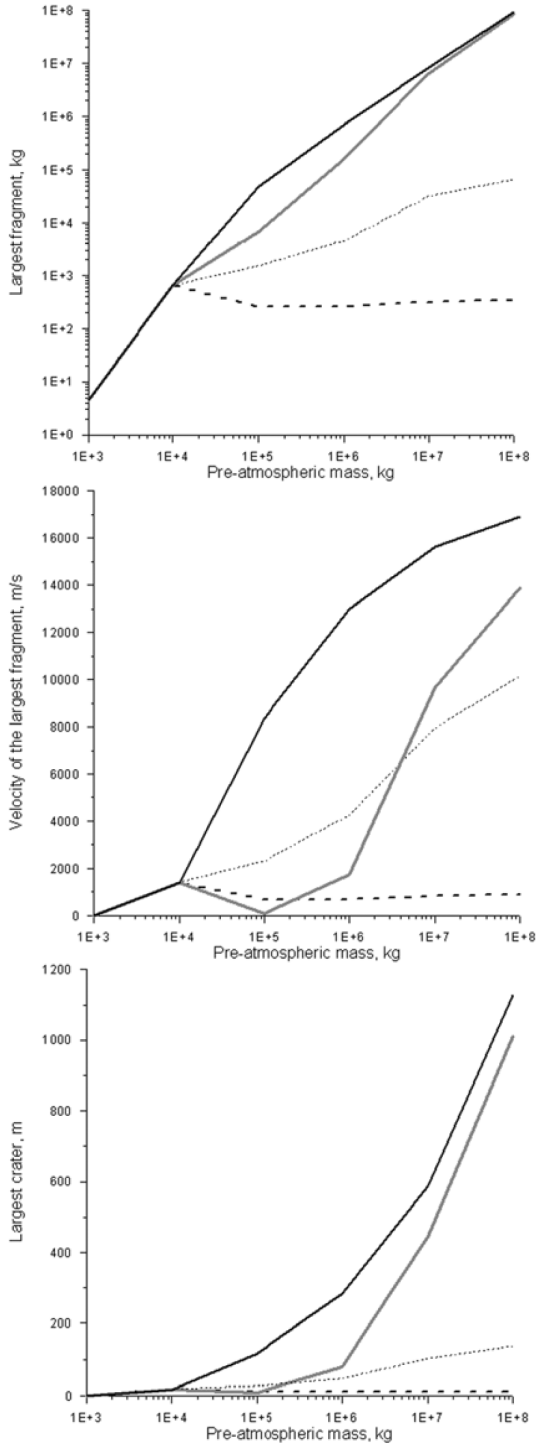

Fig. 6. The mass of the largest fragment (top), its velocity (middle), and the final crater diameter (bottom) for various pre-atmospheric iron bodies. Crater diameter applies to individual fragments, not the combined diameter of the structure resulting from multiple-fragment impact. The solid black line corresponds to entry without fragmentation (shown for reference, and certainly an overestimation). The solid gray line = fragmentation as described by the pancake model. The dashed line = regular fragmentation with Weibull statistics. The dotted line = Weibull statistics for strength with an allowed 10% deviation from the average.

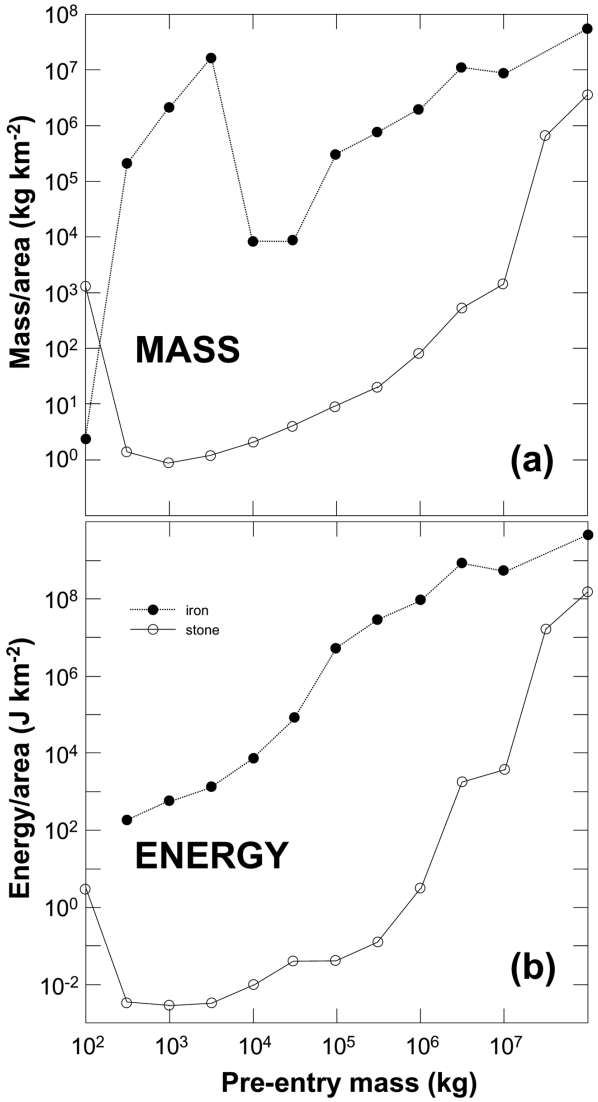

Fig. 7. The results of separated fragment model simulations for stone and iron impactors (averaged results from >1000 model simulations). The figure portrays mass (a) and energy (b) delivered to the surface per unit area for a given pre-entry mass and meteoroid type: approximate corollaries for cratering efficiency. It is apparent that, for a given pre-entry mass, irons are substantially more efficient at cratering the surface than stones.

retain a component of their cosmic velocity), this may be considered an approximate corollary of cratering efficiency. In Figs. 8a and 8b, we present data showing the ratio of final mass at the surface to pre-entry mass for stone and iron impactors (although all the material will eventually reach the surface, here we take final mass to mean fragments with velocity >20 m s^{-1} that fall as a meteorite or form a crater. 20 m s^{-1} is the precipitation free-fall velocity for cm-size fragments which may be found as meteorites). We also show the mass of the largest single fragment. Pancake model results and the (unrealistic) simple ablation curve are shown for reference.

Comparison of Model Results

Models that consider disruption clearly produce lower estimates of final mass than simple ablation models. But when pancake and SF model outputs are compared (Fig. 8), it is clear that there is also a discrepancy in terms of impactor survival. We find that estimates of total surviving material at the surface produced by both models (SF and pancake) coincide tolerably well for irons, but the same is not true for stones. A pancake model with spreading to 2× the initial radius is typically chosen, which significantly overestimates impactor survivability for stones (i.e., larger masses could reach the surface) over the whole mass range (Fig. 8). SF and pancake results only appear to converge when we consider spreading to 4× initial radius (much larger than typically used) and only for initial masses >10^7 kg, but it is not apparent if this convergence extends to masses >10^8 kg. The pancake model is not capable of providing a mass-velocity distribution for fragmented impactors, and therefore is not relevant to modeling production of terrestrial crater fields where the size of the largest crater is related to the largest surviving fragment. At larger masses (>10^7 kg), this becomes less important, possibly because larger stones behave as a liquid-like "swarm" of fragments. Pancake model results begin to converge with pure ablation results for pre-entry masses >10^{10} kg (projectile diameters 170–200 m), but until the SF approximation is capable of modeling larger stony masses, we cannot confirm that 4× spreading is the most appropriate model approximation for stony bodies in this size range. A conservative conclusion would be that atmospheric influence becomes less important for stony objects larger than 10^{10}–10^{11} kg, bodies with diameters >300 m, where the corresponding final crater size is >5 km.

Chyba et al. (1993) and others have shown that pancake models are effective in defining the altitude at which different bodies suffer catastrophic disruption. For instance, the Tunguska event is consistent with the disruption of an ~10^8 kg stony body at an altitude of ~10 km (Fig. 9). Using the SF model, we can observe the complete fragmentation behavior of a body as it penetrates further down into the atmosphere (Fig. 10). However, to predict material deposition accurately, much more complicated numerical models are needed, since small fragments are involved in a strong upward motion within the projectile wake (Shuvalov and Artemieva 2002).

The SF model enabled Artemieva and Shuvalov (1996) and Artemieva and Shuvalov (2001) to successfully reproduce the size distribution of craters and the morphology of the crater field in the Sikhote-Alin impact, and the fragmentation behavior of the Benešov bolide. It also allows us to model the formation of crater fields on Earth and other planets; model results and remote sensing observations of crater fields on Venus coincide very well (Artemieva and Bland 2003). This approach enables us to place tight constraints on impactor type, velocity, and impact angle for individual crater fields on any planet.

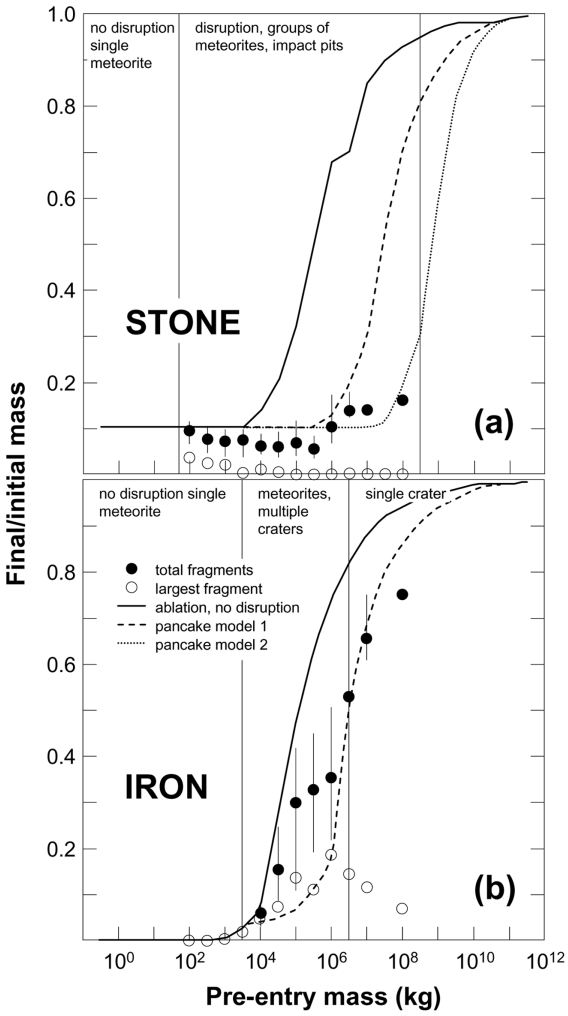

Fig. 8. The results of separated fragment, pancake, and ablation model simulations for stone and iron impactors. The figure portrays final mass (both total surviving fragments and largest single fragment) to initial mass ratio for stone (a) and iron (b) impactors. The results of pancake and ablation models are also shown: pancake model 1 is based on spreading to 2× initial radius; pancake model 2 spreading to 4× initial radius.

The SF simulations allow us to define the various styles of meteoroid fragmentation exhibited by differing impactor types and masses. Disruption is typical for stony meteorites with mass >1 kg and for iron meteorites with mass >10^3 kg. Meteoroids that are disrupted and dispersed in the atmosphere give rise to strewn fields at the surface (Figs. 11–13). For the lower mass objects, the strewn field exists as meteorite fragments, and then (with increasing mass) meteorites plus impact pits; small meter to tens of meter-size well-separated craters; craters whose rims overlap; and finally, single craters produced by a swarm of poorly separated fragments. The masses that define the transition from one type of disrupted meteoroid impact to another are indicated in Figs. 8a and 8b.

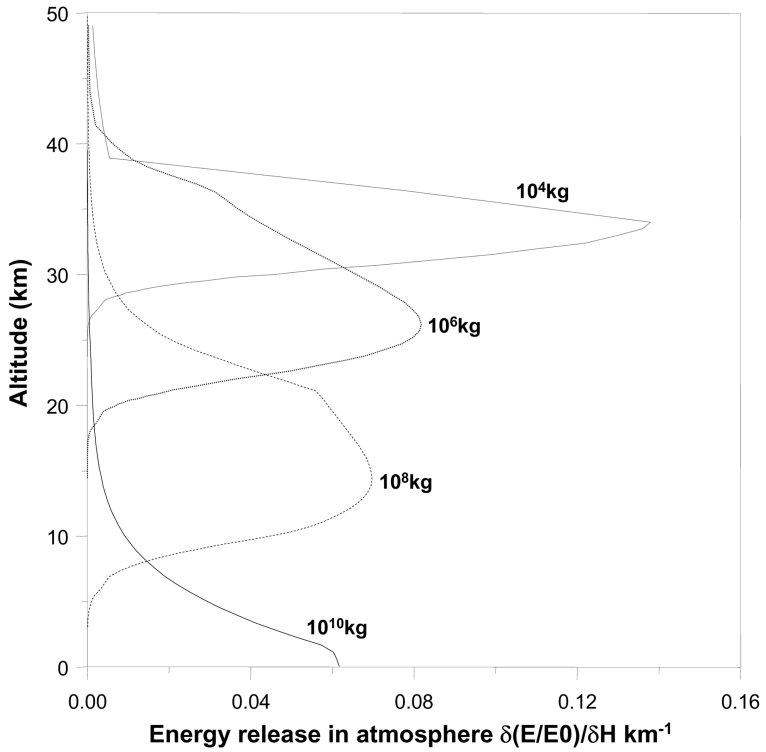

Fig. 9. Disruption altitudes for stony impactors. This figure shows the energy release in the atmosphere (δE/E0)/δH for stony bodies with mass from 10^4 kg (faint dashed curve) to 10^{10} kg (solid curve). Each maximum roughly corresponds to the height at which an asteroid explodes in the atmosphere (although, technically, asteroids do not explode. In fact, a cascade of disruption occurs when aerodynamic loading exceeds the strength of the body, with particles fragmenting into smaller particles over a short distance. Kinetic energy is transferred into heat as these particles decelerate in the atmosphere. This occurs fast enough to give the appearance of an explosion). In this figure, only the largest body (solid curve) strikes the surface with a velocity ~14 km/s. An example of a Tunguska event is ~10^8 kg (broad dashed curve), which experiences catastrophic disruption at an altitude of 10–20 km.

Bolide Fragmentation

An important outcome of the SF model simulations is the constraint they place on stony meteoroid disruption. As shown in Fig. 7 and illustrated graphically in Figs. 11 and 12, even large stony bolides fail to produce impact craters. Our modeling suggests that for stony impactors with initial mass ≤10^7 kg, the fraction of energy transferred to the surface is negligible (the model does predict rather large final masses for stones, but this parameter is acutely sensitive to the poorly known strength of stony impactors). Our simulations predict atmospheric fragmentation for much larger objects than previously thought. For stony asteroids with diameters up to a few 100 m, this means that the bulk of the energy is deposited in the atmosphere rather than at the surface, but although similarly sized irons produce single craters, fragmentation is still an issue. The largest body we have attempted to model with the SF numerical approximation is an iron impactor with a pre-entry mass of 10^{10} kg. Even for a comparatively large high-strength object such as this, we find that aerodynamic loading is sufficient to disrupt the impactor (although the fragments will hit together in a confined area and form a single complex crater of similar diameter to that which would result from the impact of a coherent projectile).

Separated Fragment Simulations and the Terrestrial Crater/ Meteorite Records

The variation in composition of the flux at the surface and fragmented body impacts predicted by the SF model are supported by an analysis of the terrestrial meteorite and cratering record. SF model simulations constrain the mass-velocity-size distribution of those fragments, allowing us to derive morphologies of simulated crater fields. In Fig. 13, we show examples of terrestrial crater fields and crater fields derived from SF model simulations. This comparison suggests that the numerical approximation of impactor fragmentation provided by the SF model bears a close resemblance to the process occurring in the terrestrial atmosphere.

SF modeling quantifies the dramatically different survivability of iron and stony impactors. Over the mass range of 10^3–10^7 kg, iron impactors transfer to the surface ~3 orders of magnitude more energy/unit area than stones: a fragmented iron impactor of 10^5 kg produces a similar crater-field to a fragmented 10^8 kg stone. Even larger stony bodies of ~10^8–10^{10} kg are much less efficient at transferring energy to the surface than the equivalent iron impactor (Fig. 7).

The SF results are in good agreement with terrestrial

crater records and also with available meteorite data. In meteorite falls, the proportion of irons increases steadily at higher masses (Fig. 14). Stony meteorites account for 96.6% of falls that are <10 kg, 92.5% of those that are 10–20 kg, 89.6% of those that are 20–50 kg, 87.1% of those that are 50–100 kg, 83.8% of those that are 100–300 kg, and 72.7% of those that are 300–1000 kg (Grady 2000). Extrapolating to larger masses suggests <5% stones for falls >4 × 10^4 kg. Small terrestrial craters are also typically associated with iron impactors. Seventeen craters with diameters <1.5 km (impactors <4 × 10^8 kg) are associated with a given impactor-type, and only one is a stone. In contrast, 18 craters >10 km have a well-defined impactor-type and 16 are stones. This suggests that in the range ~4 × 10^4 kg to 3–4 × 10^8 kg, <5% of impactors on Earth's are stones, a conclusion supported by our model simulations (Figs. 7, 8, 10, and 11). Only for pre-entry masses above ~10^{10} kg does atmospheric influence become less important, and the proportion of stony/iron impacts begins to return to normal (in this case suggesting ~10:1).

SF model simulations show that fragmented iron bolides that are <2–3 × 10^6 kg form multiple craters. Of the 22 terrestrial craters <1.5 km in diameter, 14 are <0.3 km. Nine of these are multiple craters, while none of the 0.3–1.5 km craters are multiples, suggesting that iron impactors <3 × 10^6 kg are disrupted at sufficient altitude so that separated fragments form multiple craters. However, it is interesting that for iron bolides that are >10^7 kg, the SF model indicates that the impact of closely spaced separated fragments will form single simple craters (this would also be true of stony bolides probably greater than approximately 10^{10}–10^{11} kg). This idea was originally suggested by Melosh (1981). Fragmentation is the norm, even when single craters are produced, until we get into the regime of km-size impactors (see previous discussion).

Confirming that small single craters on Earth have been produced by separated fragments is difficult. For iron impactors between ~10^7–10^9 kg (where some separation occurs between fragments even though a single crater is produced from a fragmented impactor), we might anticipate that the ratio of true crater depth to crater diameter (d_t/D) would be lower than if the projectile remained intact (Schultz and Gault 1985). The d_t/D of simple terrestrial craters has been estimated from geophysical measurements and drilling (Earth Impact Database 2002). We note that simple craters of intermediate size tend to have low d_t/D. However, with the exception of Lonar (0.052 Ma and d_t/D of 0.246), these craters are old (>40 Ma) and will have experienced significant modification. An environment where atmospheric disruption of large impactors occurs but erosive modification of craters is limited is that of Venus (McKinnon et al. 1997). Although not directly comparable to the Earth (a denser atmosphere means disruption of larger bodies), the smallest craters on Venus have anomalously low d_t/D ratios (Moore et al. 1993; McKinnon et al. 1997; Herrick and Lyons 1998; Cochrane 2002).

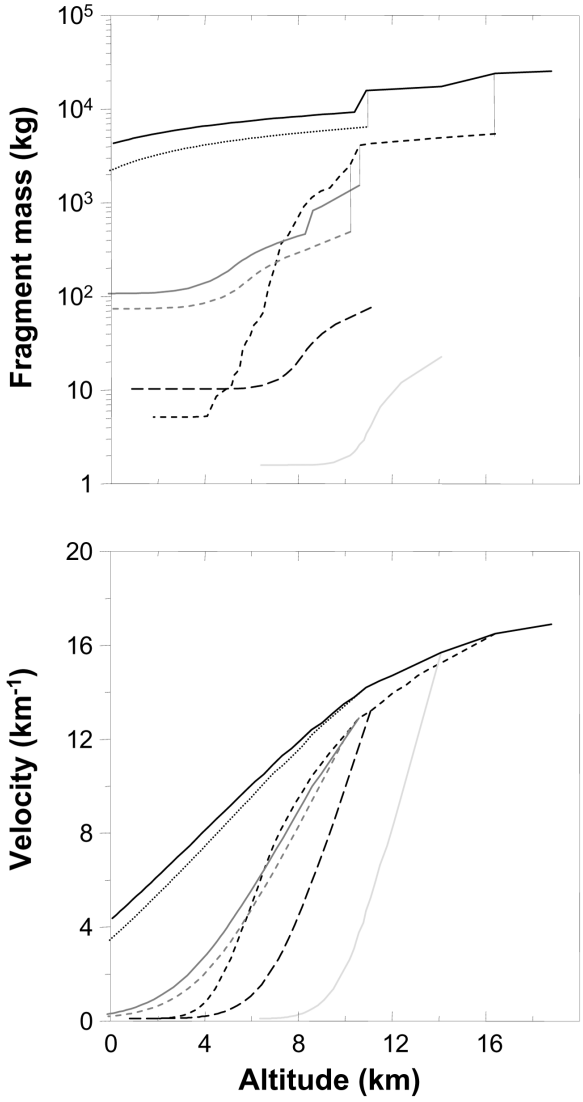

Fig. 10. The mass (top) and velocity (bottom) of iron fragments disrupted in the atmosphere. This figure traces the evolution of a given fragment down into the atmosphere. Different fragments are represented by different shades or dashes. The first disruption occurs at an altitude of 16 km. Smooth decreases in mass are due to ablation; sharp ones (vertical lines in the upper plate) are due to fragmentation.

The correspondence between SF model results and the available meteorite and cratering data suggests that we can be confident in the model predictions for the atmospheric behavior of small bolides. The results of our simulations therefore provide us with a template for understanding the atmosphere-bolide interaction for a range of pre-entry masses and impactor types. With a knowledge of the overall flux and the composition of the flux at the upper atmosphere, we can use our simulations to calculate the mass flux (both combined mass of all fragments >100 g, and the largest surviving

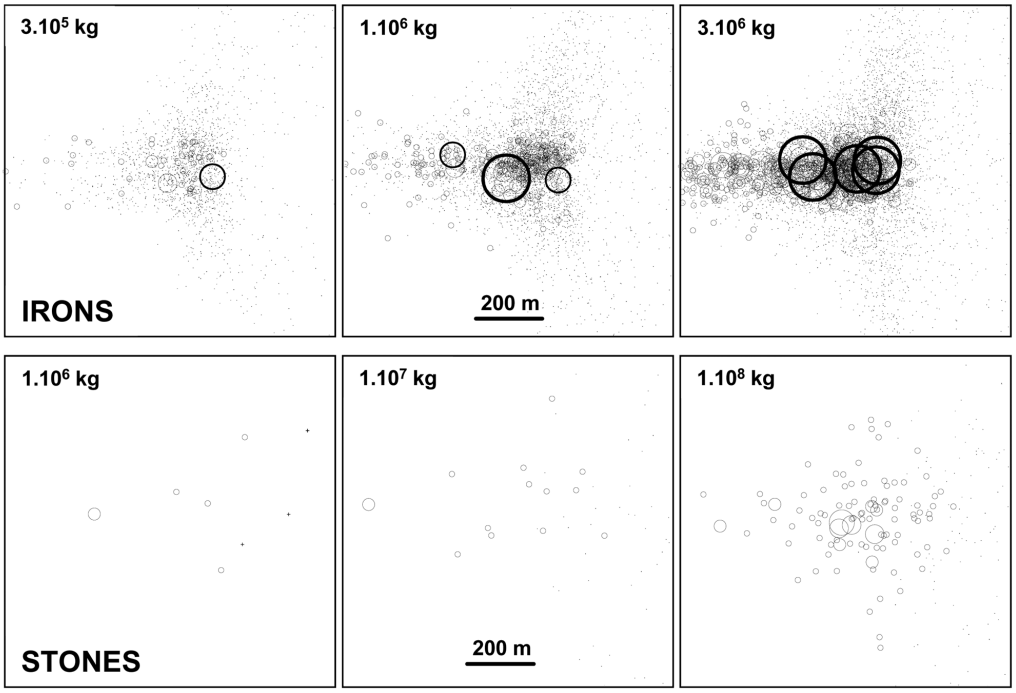

Fig. 11. Strewn fields for iron (top row) and stony (bottom row) bodies for a range of pre-entry masses. Each square shows the 1 × 1 km area where the largest craters are found (the total strewn field size may be 10 × 20 km). Sizes of circles approximately equal the size of impact craters. Dots indicate <10 m pits. The first plate for iron meteorites roughly corresponds to the Sikhote-Alin iron shower (the last plate would probably be identified as a single joint crater). For stony bodies, although a small percentage of the impactor may reach the surface, even a 10^8 kg mass does not lead to impact crater formation.

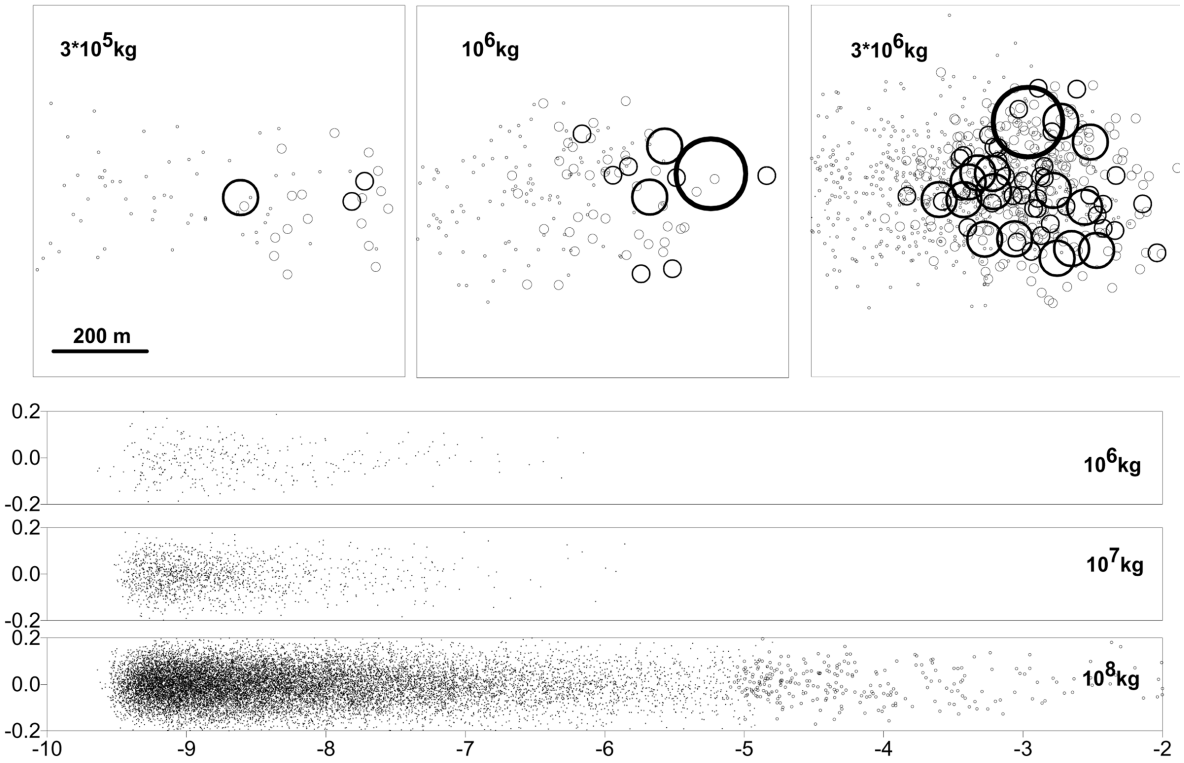

Fig. 12. Strewn fields for various initial masses of iron asteroid (three upper plates) and of stony asteroids (elongated bottom plates). Stony asteroids of 10^8 kg do not produce craters, but rather a swarm of meteorites.

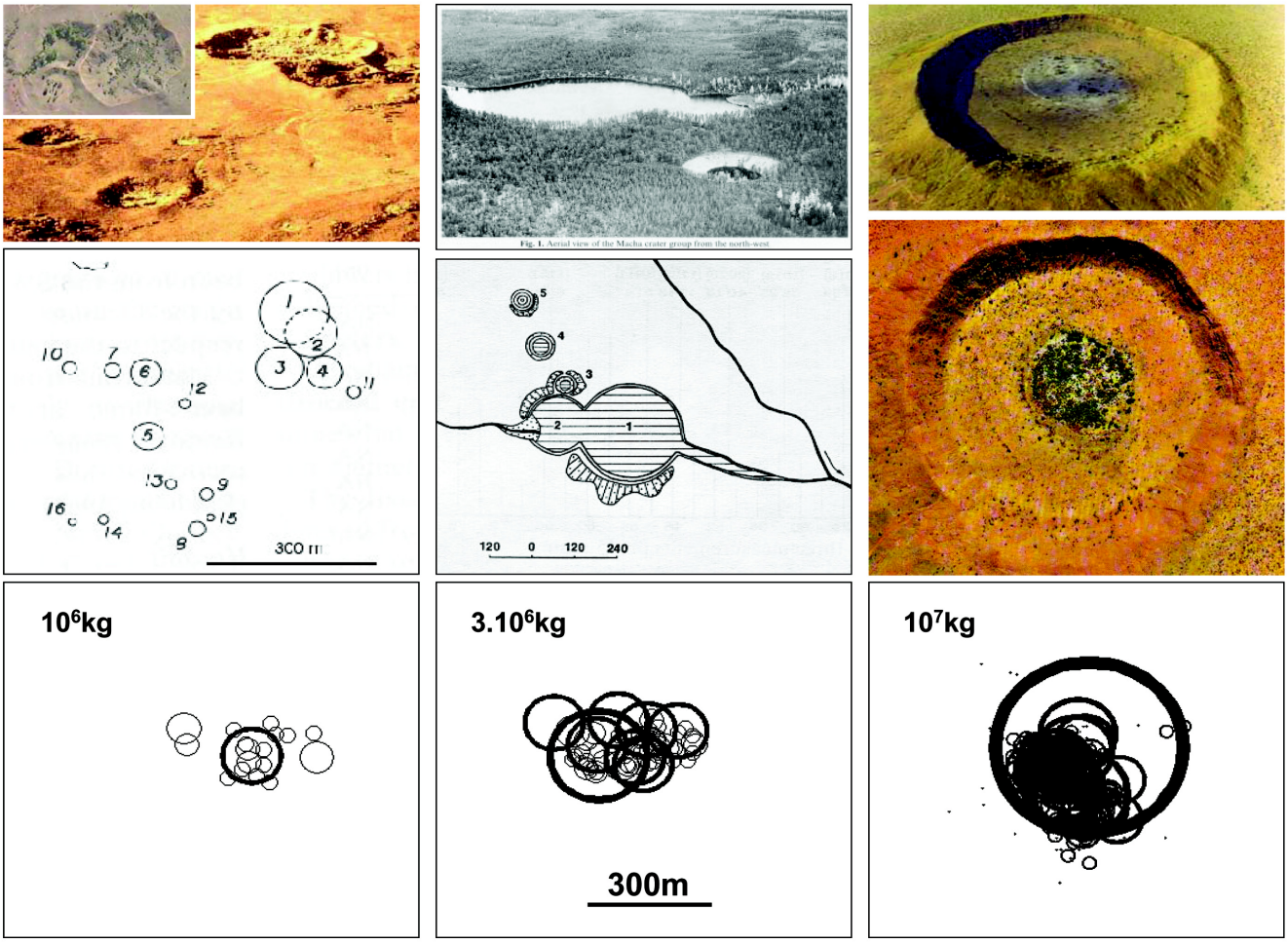

Fig. 13. A comparison of SF model simulations and terrestrial crater fields. The figure shows the transformation of a strewn field into an irregular crater, and then into a single crater as pre-atmospheric mass increases. The left column shows the Henbury craters in Australia with at least 15 separate or overlapping craters, the largest of which is 147 m (Milton 1972). The middle column shows the Macha crater field in Russia, with two overlapping craters (300 m and 180 m) and three smaller craters (Gurov 1996). The right-hand column shows the 0.45 km diameter Amguid crater in Algeria and the 0.875 km Wolfe Creek crater in Australia. The bottom row illustrates the results of numerical simulations for the 30° impact of iron bodies with masses ranging from 10^6 kg to 10^7 kg.

fragment) at the Earth's surface. But first we must define the size-frequency distribution of impactors at the upper atmosphere and constrain their composition.

FLUX AND COMPOSITION OF IMPACTORS AT 1 AU

Size-Frequency Distribution

The cumulative size-frequency distribution (SFD) of the impactor population can be used as a probe of composition, as well as a means of assessing any temporal variation in the source of impactors. The lunar mare provide a record of the impactor SFD, averaged over ~3.5 Ga (Hartmann et al. 1981; Heisinger et al. 2003), and have been used as a calibration point for dating surfaces by crater counting throughout the inner solar system (e.g., Hartmann 1967; Hartmann 1970; Neukum et al. 1975; Neukum and Wise 1976; Hartmann 1977; Hartmann et al. 1981; Hartmann 1999; Hartmann and Neukum 2001). The shape of the SFD derived from lunar surfaces of a variety of ages shows little variation (Neukum and Ivanov 1994), suggesting that the distribution is stable (within approximately a factor of 2) over the last ~3 Ga. The youngest cratered surfaces on Mars also show a very similar crater SFD (Hartmann 1999). The lunar mare SFD suggests a collisionally processed population (Dohnanyi 1969; Bottke et al. 2005). Neukum et al. (2001), Werner et al. (2002), and Ivanov et al. (2003) have converted the lunar mare crater SFD to an impactor SFD and found a close match to the SFD of main belt asteroids and NEOs. Bottke et al. (2005) have also investigated the formation of the main belt SFD using a collisional evolution model. Their results suggest that the primordial main belt experienced a brief but intense period of collisional processing, soon after planetary embryo formation. The asteroid belt experienced as much

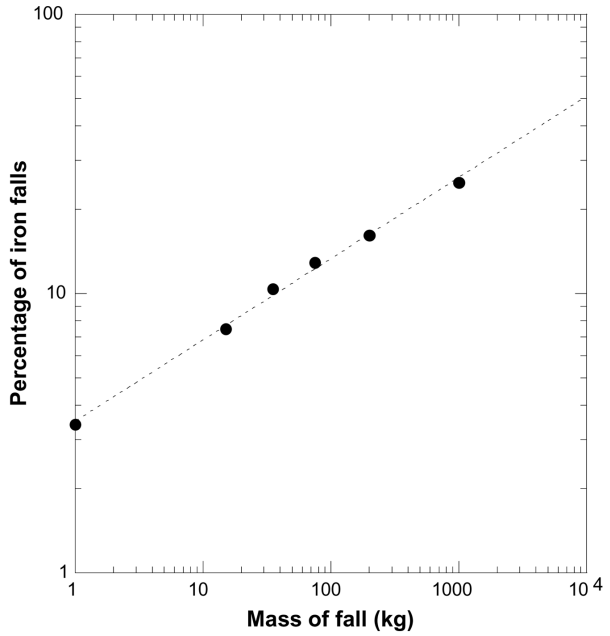

Fig. 14. The proportion of iron meteorite falls against mass. Data are binned for 1–15 kg falls, 15–35 kg, 35–75 kg, 75–200 kg, and 200–1000 kg. The number of irons as a proportion of total falls increases, approximately as a power law, from 3.4% in the 1–15 kg bin to 25% in the 200–1000 kg bin.

comminution during this initial period as it has over the rest of the solar system history (Bottke et al. 2005). Bottke et al. (2005) consider the "structure" in the asteroid SFD to be a relic of this early violent period, with most asteroids $D \geq 120$ km being primordial and smaller objects being the products of fragmentation events.

Recently, questions have been raised on the applicability of a simple lunar mare (and Martian) small-crater SFD for chronology, with the suggestion that small secondaries have biased the crater population (Plescia 2005; McEwen et al. 2005; Bottke et al. 2005). If we were to use a scaled mare SFD to help constrain the shape of the impactor SFD at the Earth, the presence of secondaries would have the effect of leading us to overestimate the number of small impactors in the population. We return to this issue in the following section.

Impact Rates at the Upper Atmosphere

Over recent years, the impactor flux for the upper atmosphere has been well-constrained over specific portions of the mass distribution: ground-based camera network observations of meteoroid fireballs (Halliday et al. 1996); radiation energies of bright flashes from the disintegration of large meteoroids measured from geostationary satellites (Nemtchinov et al. 1997; Brown et al. 2002); acoustic detection of large bolides (ReVelle 1997); telescopic observations and modeling of the NEO population (Rabinowitz et al. 2000; Stuart 2001; Morbidelli et al. 2002; Harris 2002); and the data set of large terrestrial craters (Grieve and Shoemaker 1994; Hughes 1999, 2000) (objects $>10^{12}$ kg transit the atmosphere with little effect so final mass is similar to initial mass). A compilation of this data is shown in Fig. 15, converted to impactor mass (see earlier discussion for details).

Brown et al. (2002) noted that the SFD of meteoroids and small NEOs at the top of the atmosphere may be fitted to single power law over ~9 orders of magnitude, up to bodies of $\sim 10^{10}$ kg (200 m stony projectile), corresponding to an ~3 km diameter crater. However, it is clear that a single power law is not sufficient to fit the SFD of impactors over a larger size range. Does a scaled lunar mare production function provide an adequate fit? As we have seen, Neukum et al. (2001), Werner et al. (2001), and Ivanov et al. (2003) have demonstrated that the overall shape of the NEO and Main Belt asteroid mass distribution (Rabinowitz et al. 2000; Stuart 2001; Morbidelli et al. 2002), and the slope of the meteoroid data (Nemtchinov et al. 1997), is similar to the cumulative SFD of lunar mare craters (the Neukum or Hartmann Production Functions—NPF or HPF). Fitting the upper atmosphere data using a scaled HPF and NPF, we find that over a $1–10^{16}$ kg mass range the fit is adequate; although there is significant divergence in the intermediate-mass material (the HPF and NPF curves underestimate this portion of the flux). Instead, and for the rest of this paper, we model the upper atmosphere SFD using a series of power law branches, each branch is a best fit to the available data in that mass range:

$$\log N = -0.480 \log m + 4.568, \; m < 3 \text{ kg}$$
$$\log N = -0.926 \log m + 4.739, \; 3\text{kg} < m < 1.7.10^{10} \text{ kg}$$
$$\log N = -0.373 \log m - 0.922, \; 1.7.10^{10} \text{ kg} < m < 3.3.10^{12} \text{ kg}$$
$$\log N = -0.454 \log m + 0.086, \; 3.3.10^{12} \text{ kg} < m < 8.4.10^{14} \text{ kg}$$
$$\log N = -0.672 \log m + 3.352, \; m > 8.4.10^{14} \text{ kg}$$

At the large impactor end, we take an average of the Grieve and Shoemaker (1994) and Hughes (1999, 2000) terrestrial crater data as a guide. The overall curve (Fig. 15) is a close fit to virtually all the data for the upper atmosphere.

Regarding the question of abundant secondaries biasing the small crater portion of the HPF and NPF, from this comparison of upper atmosphere data and the mare crater SFD (converted to impactor mass) it appears that the HPF and NPF curves underestimate the number of small crater-forming objects. This is the reverse of what we would expect if these functions were strongly biased by abundant secondaries.

Flux estimates for the upper atmosphere derived from our best-fit curve are shown in Table 1. These estimates are in general slightly higher than those presented by Bland and Artemieva (2003). The difference is rather small (on average, less than a factor of two), and arises from the adoption in this work of an unconstrained best fit to the upper atmosphere

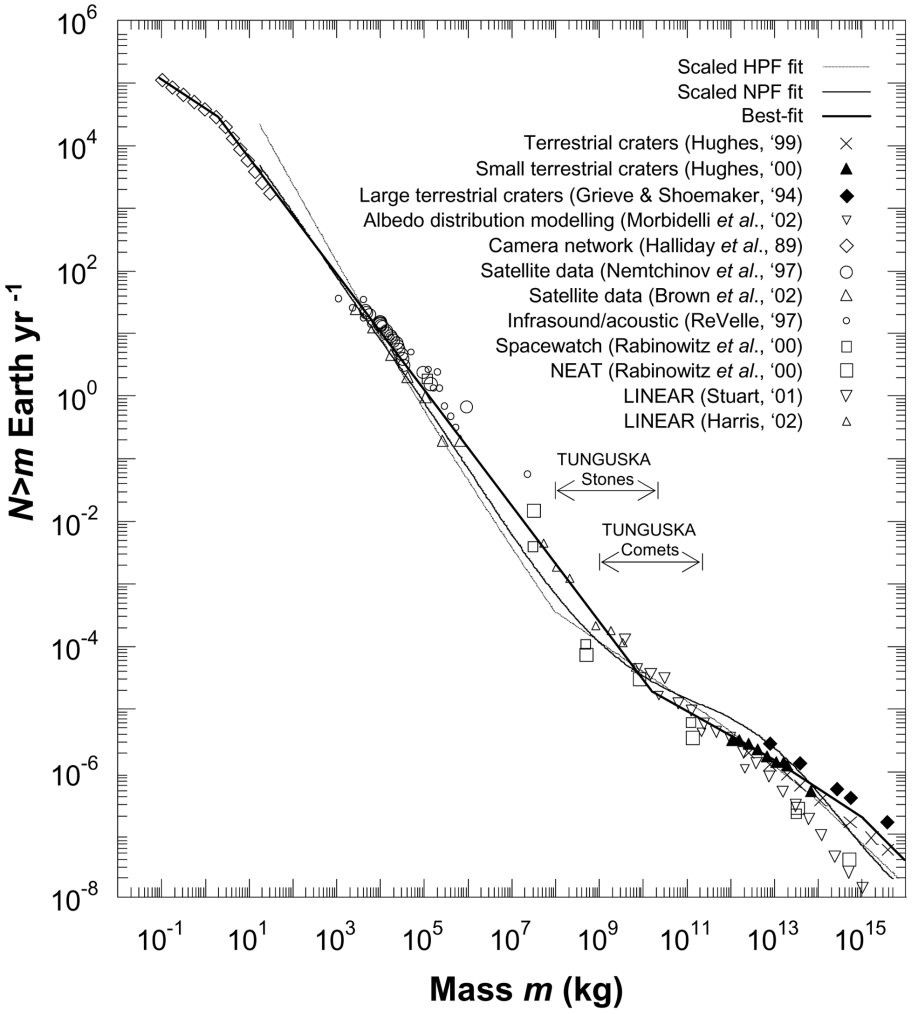

Fig. 15. A compilation of impact rate estimates for the upper atmosphere. Impactor flux is expressed in terms of number of events *N* greater than mass *m* per year at Earth. Unmodified Hartmann and Neukum Production Functions (HPF and NPF), derived from the lunar mare crater record (Hartmann 1999; Ivanov et al. 2003) and scaled to impactor mass using Schmidt and Housen (1987), are scaled to fit the upper atmosphere data. We also show our best fit to the upper atmosphere data composed of a series of power laws. The mass range within which we might expect Tunguska-like events (for stony and cometary impactors) is also indicated.

data, rather than the use of a scaled HPF/NPH curve (as in Bland and Artemieva 2003). In deriving a surface impact production function, we scale the upper atmosphere curve based on our modeling results, so this difference is also passed on to flux estimates at the Earth's surface.

The significance of the curvature in the SFD for estimating terrestrial impact rates does not appear to have been recognized in some earlier studies (e.g., Ward 2002). Over much of the mass distribution, our fit to the recent upper atmosphere data suggest a lower flux than previous estimates (Chapman and Morrison 1994; Morrison et al. 1994; Ward and Asphaug 2000; Ward 2002).

Stony bodies $>10^8$ kg can penetrate low enough in the atmosphere prior to disruption to affect the surface (Figs. 7 and 8), so a fit to the upper atmosphere data for bodies larger than 10^8 kg defines the approximate rate at which Tunguska-like events will occur. Brown et al. (2002) estimated the rate of these events at approximately one every 1000 years. Our best fit to all the upper atmosphere data suggests an interval of ~500 years between Tunguska events (see Fig. 15 and Table 1). Given the assumptions involved, these estimates are essentially identical.

The Composition of the Impactor Flux at 1 AU

There are clearly a wide range of materials arriving at the Earth's upper atmosphere, but in terms of their physical properties they can be effectively subdivided into three broad groups: stony material derived from stony bodies or from the crust of differentiated bodies, iron material derived from the core of differentiated asteroids, and cometary material. We have not included comet entry modeling in our SF simulations. Obviously, they are weaker than stony bodies (see for example Chyba et al. 1993) and hence are incapable

Table 1. Flux estimates for the upper atmosphere, based on our best-fit to the upper atmosphere data set composed of a series of power laws. The data are presented as number of events per year for the Earth above a given mass. The interval in years between events of a given mass is also shown, as is the energy of each event (following Brown et al. 2002).

Mass (kg)	Energy (kt)	Frequency ($N > m\ yr^{-1}$)	Interval yr (1/N)
0.1		111,800	
0.5		51,630	
1		37,020	
5		12,350	
10		6497	
50		1463	
100		770	
500		173	
1000	0.042	91	
5000	0.210	21	
10,000	0.421	11	
50,000	2.10	2.4	
100,000	4.21	1.3	
500,000	21.0	2.89E − 01	3.5
1,000,000	42.1	1.52E − 01	6.6
5,000,000	210	3.42E − 02	29
1.00E + 07	421	1.80E − 02	56
5.00E + 07	2103	4.06E − 03	246
1.00E + 08	4205	2.14E − 03	468
5.00E + 08	21,025	4.81E − 04	2079
1.00E + 09	42,050	2.53E − 04	3951
5.00E + 09	210,250	5.70E − 05	17,540
1.00E + 10	420,500	3.00E − 05	33,340
5.00E + 10	2,102,500	1.22E − 05	82,080
1.00E + 11	4,205,000	9.41E − 06	106,300
5.00E + 11	2.10E + 07	5.16E − 06	193,800
1.00E + 12	4.20E + 07	3.98E − 06	251,000
5.00E + 12	2.10E + 08	2.12E − 06	472,800
1.00E + 13	4.21E + 08	1.54E − 06	647,400
5.00E + 13	2.10E + 09	7.44E − 07	1,344,000
1.00E + 14	4.20E + 09	5.43E − 07	1,840,000
5.00E + 14	2.10E + 10	2.62E − 07	3,819,000
1.00E + 15	4.20E + 10	1.84E − 07	5,434,000
5.00E + 15	2.10E + 11	6.24E − 08	16,040,000
1.00E + 16	4.21E + 11	3.91E − 08	25,560,000
5.00E + 16	2.10E + 12	1.33E − 08	75,440,000
1.00E + 17	4.20E + 12	8.32E − 09	120,200,000
5.00E + 17	2.10E + 13	2.82E − 09	354,900,000

of cratering the surface at least for the 10^2–10^9 kg mass range. Moreover, crater counts on Jupiter's satellites (Zahnle et al. 2003) clearly show a deficiency of small comets. Thus, the iron:stone ratio is more relevant to our estimate of the flux at the surface for masses less than ~10^{10} kg. However, the asteroid:comet ratio may be significant in assessing the frequency of Tunguska-like events over the 10^8–10^{12} kg mass range and in defining the temporal variability in the flux of larger bodies. We modeled a comet entry with the pancake model and received results similar to Chyba et al. (1993), i.e., 10^{10}–10^{12} kg cometary bodies do not reach the Earth's surface but deposit their energy in the upper atmosphere.

It is interesting to note that the evidence from large terrestrial craters indicates a higher mass flux than would be deduced from the NEO dataset. It would be premature to overinterpret this, but the divergence appears to be real. There are a number of possible explanations—some of which would put the true flux closer to that suggested by the NEO data, and some in support of the crater data. First, the estimated mass of an impactor varies significantly depending on which crater scaling law is chosen. Converting craters from their present diameter to a transient diameter (properly accounting for crater collapse) and then to a projectile size involves a number of assumptions. It is possible that current crater scaling laws overestimate impactor mass. A second explanation would be that a non-NEA population (presumably comets) contributes to the numbers of large terrestrial impactors. Thirdly, if the lifetime of an NEA is less than the time it takes to produce another NEA of the same size, the real presence "in the sky" of this size body will oscillate between 0 and 1. The lack of astronomically observed NEAs of a large size at the current time does not necessarily mean that they never appeared. Craters on the moon and Earth are accumulated for 10-100-1000 million years; the time scale of the asteroids on Earth crossing orbits is 1–3 (up to a maximum of ~30) million years. Hence, it is possible that the population of impactors originating as NEAs is larger than the current snapshot we have of the NEA population. Unfortunately, it is beyond the scope of this paper to discriminate between these possibilities, but it should be noted that an uncertainty remains in flux estimates for higher mass objects.

On a related point, it is noteworthy that those advocating a periodicity in the impact record (e.g., Napier and Clube 1979; Rampino and Stothers 1984; Raup and Sepkoski 1984; Rampino and Haggerty 1994; Napier 1998) require that a majority of large terrestrial craters were formed by comets. We will consider evidence of possible cometary impact in more detail below.

Size-Frequency Distribution of Comets and Asteroids

As we have seen, the size-frequency distribution of collisionally processed materials is quite distinctive. Hughes (1994) compared the SFD of comets and asteroids and found that cometary impactors formed <5% of craters >20 km in diameter. As discussed above, Neukum, Ivanov, and Hartmann (2001), Werner et al. (2002), and Ivanov et al. (2003) have shown that the projectile SFD derived from lunar craters is close to the SFD of Main Belt asteroids and the current NEO population. The implication is that comets have contributed only a minor portion of the overall flux recorded by the lunar mare. However, this conclusion is based on the assumption that comets are not collisionally processed bodies.

Modeling the Production of Comets in the Inner Solar System

Attempts at modeling the flux of comets at 1 AU have produced a large range in estimates of the asteroid:comet ratio. Bailey and Stagg (1988) suggested that only 2% of terrestrial craters are cometary. Shoemaker et al. (1990) compared the population of known NEAs and active Earth-crossing comets and suggested that 24% of craters >20 km were formed by comets, and 85% of the craters >100 km. Shoemaker (1998) revised this estimate upward to 50% of craters >20 km and 100% of craters are >100 km. Weissman (1990) used estimates of the population of the Oort Cloud and historical data from observations of short and long period comets, and estimated that 28% of craters >10 km were formed by comets (with H = 16.8 for LP comets, 15.4 for SP comets). Bailey and Emel'Yanenko (1998) estimated that inert Halley-type comets impact the Earth producing 20 km craters every 200–300 ka. As the terrestrial crater population constrains the overall rate of impacts of this size rather well at between one every 350 ka (Grieve and Shoemaker 1994), 435 ka (Shoemaker and Shoemaker 1990), or 560 ka (Hughes 2000), this estimate would suggest that 100% of craters >20 km are formed by comets and that many of those craters remain undiscovered, even on stable cratons. In contrast, Levison et al. (2002) showed that the population of dormant Halley-type comets is actually much lower, due to progressive physical disruption. They calculated that Halley-type comets with $H < 18$ should impact only once every 780 Ma.

Spectral Properties of NEOs

Although NEOs appear to show a greater spectral diversity than Main Belt asteroids (Binzel et al. 2001), they are also a closer match to the meteorite population. With decreasing size and younger surfaces (smaller objects have shorter collisional lifetimes), NEOs show a transition in spectral properties to more resemble the most common meteorites—the ordinary chondrites (Binzel et al. 2003). Evidence suggests that comets contribute, at most, only a few percent of the NEO population (Binzel et al. 2003).

Geochemical Evidence for the Nature of the Impactor

Studies of terrestrial impact melts, particularly recent advances in Cr-isotope and PGE analyses, which allow quite specific determination of impactor type, constitute ground-truth evidence on the composition of the flux. The composition of the melt sheet in the 70 km diameter Morokweng crater in South Africa has recently been analyzed in great detail in an attempt to define the impactor type. Shukolyukov et al. (1999) used Cr isotopes to show that the impactor was an ordinary chondrite, and the Cr/Ir ratio to suggest that it was an L-group ordinary chondrite. Subsequent additional PGE analyses (McDonald et al. 2001) broadly supported this interpretation, suggesting an L or LL chondrite impactor. Similarly, PGE ratios in samples of the Clearwater East impact melt (McDonald 2002) and Cr-isotope data (Shukolyukov and Lugmair 2000) indicate that the twin Clearwater structures (the 26 km Clearwater East, and 36 km Clearwater West) were formed by an ordinary chondrite impactor. Chromium isotopes also suggest that the Chicxulub impactor was a carbonaceous chondrite (Shukolyukov and Lugmair 1998), which appears to be supported by the discovery of a highly weathered fragment of chondritic meteorite in a DSDP core, showing affinities to either CO, CV, or CR chondrites (Kyte 1998). Finally, evidence from the oldest impact deposits on Earth, the spherule beds in the Barberton Greenstone Belt of South Africa, suggest that these too may have been produced by impact of a large (>20 km diameter) carbonaceous chondrite body, most likely of CV composition (Shukolyukov et al. 2000).

Ordinary chondrites certainly have an asteroidal origin, and it is very likely that carbonaceous chondrites also originate from the asteroid belt. Taken together, although these data represent a rather small number of craters, they are important as they suggest that asteroidal material is an important component of the large impactor flux.

Proportion of Iron Impactors at the Upper Atmosphere

Although there is a wide range of estimates for the proportion of comets, the ratio of irons to stones at the upper atmosphere can be inferred from NEO and Main Belt asteroid spectroscopy, meteorite composition, and impactor types in large terrestrial craters (Burbine 2002). Assuming that iron asteroids are within the X-class, spectroscopy places upper limits on the abundance of irons amongst Main Belt asteroids (Bus and Binzel 2002) (~8%) and NEOs (Binzel et al. 2003) (~10%). If we only consider M-class asteroids (a sub-type within the X-class), the proportions are ~5% of Main Belt asteroids (Tholen 1989) and ~2% of NEOs (Binzel et al. 2003). However, it should be noted that a number of M-class asteroids show absorption features in their infrared spectra which indicate that they are not metallic. In terrestrial impacts, of the ~20 craters >10 km that have been associated with a given impactor type, two were apparently formed by irons (Koeberl 1998). Considering the population of meteorite falls, and including only those < 10 kg in mass (to minimize the effect of the atmosphere in screening out stones—see Fig. 14), the proportion of irons is 3.4%.

Given the above, it seems reasonable to suppose that the terrestrial impactor population is dominated by asteroids, and has remained broadly stable in terms of composition and size-frequency distribution over geological time. There is no evidence to suggest that comets comprise more than a minor fraction (<10%) fraction of the small impactor (<20 km diameter craters) population, and the evidence for them contributing a significant portion of large impactors is equivocal. Based on the NEO spectral data, composition of impactors in terrestrial craters, and the composition of meteorites, for the purposes of this study, we will take the proportion of iron impactors at the upper atmosphere to be 5% ± a factor of two.

FLUX AT THE EARTH'S SURFACE

We now scale the curve for the upper atmosphere flux to an impact rate at the Earth's surface. Over the mass range 2×10^4–1×10^8 kg (bodies producing craters of ~0.05–1 km in diameter) our SF modeling constrains the fraction of a given impactor that reaches the surface with high energy. The terrestrial data and the SF model simulations suggest that the overwhelming majority of these bodies are iron impactors (Figs. 7, 8, 10, and 11). So an impact rate at the surface may be estimated by scaling the flux at the top of the atmosphere using the I:S ratio (×0.05, assuming negligible stony impactors at the surface) and the calculated final mass derived from ~400 SF model simulated iron bolide impacts over this mass range. Our flux estimates, based on data for the total mass of high velocity fragments and the largest fragment, are shown in Fig. 16.

Given that the terrestrial data supports an iron-dominated impactor population over the 4×10^4–4×10^8 kg mass range, we suggest that a flux curve intermediate between the largest iron fragment and total high velocity iron fragments is most appropriate over this mass range. But the relative contribution of largest fragment and total terminal mass to crater size changes over this mass interval. Over the ~10^4–3×10^6 kg range (3×10^6 kg corresponds to an iron impact forming a 0.3 km crater), largest fragment size is most significant (impactors in this mass range form crater fields, with the largest crater resulting from an impact of the largest fragment). Over the 3×10^6–4×10^8 kg range fragmented impactors strike together to form single craters (crater diameter >0.3 km), so at the upper end of this mass range the total impacting terminal mass is most significant. Within the confines of our SF modeling results, we adopt a curve intermediate between the largest single fragment and total terminal mass data at the lower end, and coincident with the total terminal mass of iron impactors at the upper end of this mass range.

As noted, the terrestrial crater record is incomplete over this mass interval, and our resulting curve predicts a significantly higher flux than would be deduced from the terrestrial crater data set. However, if we select recent (<0.05 Ma) small (<1 km) impacts in Australia (Shoemaker and Shoemaker 1988), an area where arid conditions limit erosion and obscuring vegetation is minimal, we observe a close match to our modeled iron-impactor flux estimate for bodies ~10^5 kg (see Fig. 16). For objects <10^5 kg, the Australia data depart from our modeled curve. However, even minimal erosion would reduce craters <100 m in diameter to anonymous shallow depressions: it is reasonable to suppose that many such craters have gone unrecognized.

Where we have data on the ratio of iron to stony impactors at the Earth's surface, it is sensible to use it. Over the mass range for which we have samples, the proportion of iron meteorites increases in a simple power law relationship with increasing mass (Fig. 14). For 10–10^3 kg bodies at the surface, we therefore scale our SF model results for total surviving meteorite-sized fragments based on the best fit to the upper atmosphere data, taking into account the decreasing proportion of stone meteorite falls of 1–10^3 kg. This curve (see Fig. 16) is therefore based on SF results, upper atmosphere data, and the observed depletion of stony meteorites. However, we can also arrive at an approximate curve by simply extrapolating from fireball data for small meteorites on the ground (a power law with slope –0.82) (Halliday et al. 1989). As shown in Fig. 16, these curves are coincident.

Modeling separated fragments becomes unwieldy for objects >10^8 kg. However, SF and pancake model (4× spreading) estimates of final mass for initial bodies >10^7 kg appear to show some convergence (Fig. 8): Our data indicate these objects occur as a closely separated liquid-like "swarm" of fragments at the surface. We therefore scale our best-fit upper atmosphere curve to a surface flux using pancake model (4× spreading) results for objects >10^8 kg, and a varying *I:S* ratio based on the observed depletion in craters formed by stony impactors over the 1.5–10 km crater interval (impactor masses of ~3.9×10^8–5.3×10^{11} kg). In the small crater data, almost all the craters <1.5 km in diameter were formed by irons. This is not because stony meteorites have been eroded from these craters: Of the 22 craters known with diameters <1.5 km, a full 17 have a confirmed impactor type, and 16 of those were formed by iron or stony iron objects. The only case of a chondritic impactor is Tswaing crater in South Africa (1.13 km). Based on this, we can constrain the I:S ratio for impactors in the 3.9×10^8–5.3×10^{11} kg mass range. We assume 95% iron impactors forming craters <1.5 km diameter, with a return to the "normal" ratio of 95% stones forming craters >10 km diameter.

Our estimate for a complete surface impactor production function for Earth, as discussed above, is a series of power-law branches, partly reflecting structure in the initial pre-entry SFD and partly structure imposed by atmospheric fragmentation:

$\log N = -0.492 \log m + 3.646$, $m < 1$ kg
$\log N = -0.820 \log m + 3.648$, $1 \text{ kg} < m < 10$ kg
$\log N = -1.250 \log m + 4.098$, $10 \text{ kg} < m < 2.4 \times 10^3$ kg
$\log N = -0.996 \log m + 2.983$, $2.4 \times 10^3 \text{kg} < m < 3.1 \times 10^6$ kg
(0.3 km crater)
$\log \mathrm{N} = -0.486 \log m - 0.330$, $3.1 \times 10^6 \text{kg} < m < 3.9 \times 10^8 \text{kg}$
(1.5 km crater)
$\log N = -0.253 \log m - 2.326$, $3.9 \times 10^8 \text{ kg} < m < 5.3 \times 10^{11}$ kg
(10 km crater)
$\log N = -0.373 \log m - 0.922$, $5.3 \times 10^{11} \text{ kg} < m < 3.3 \times 10^{12}$ kg
(16 km crater)
$\log N = -0.454 \log m + 0.086$, $3.3 \times 10^{12} \text{ kg} < m < 8.4 \times 10^{14}$ kg
(67 km crater)
$\log N = -0.672 \log m + 3.352$, $m > 8.4 \times 10^{14}$ kg

The complete flux curve at the Earth's surface is shown in Fig. 16, compared to our best fit to the upper atmosphere

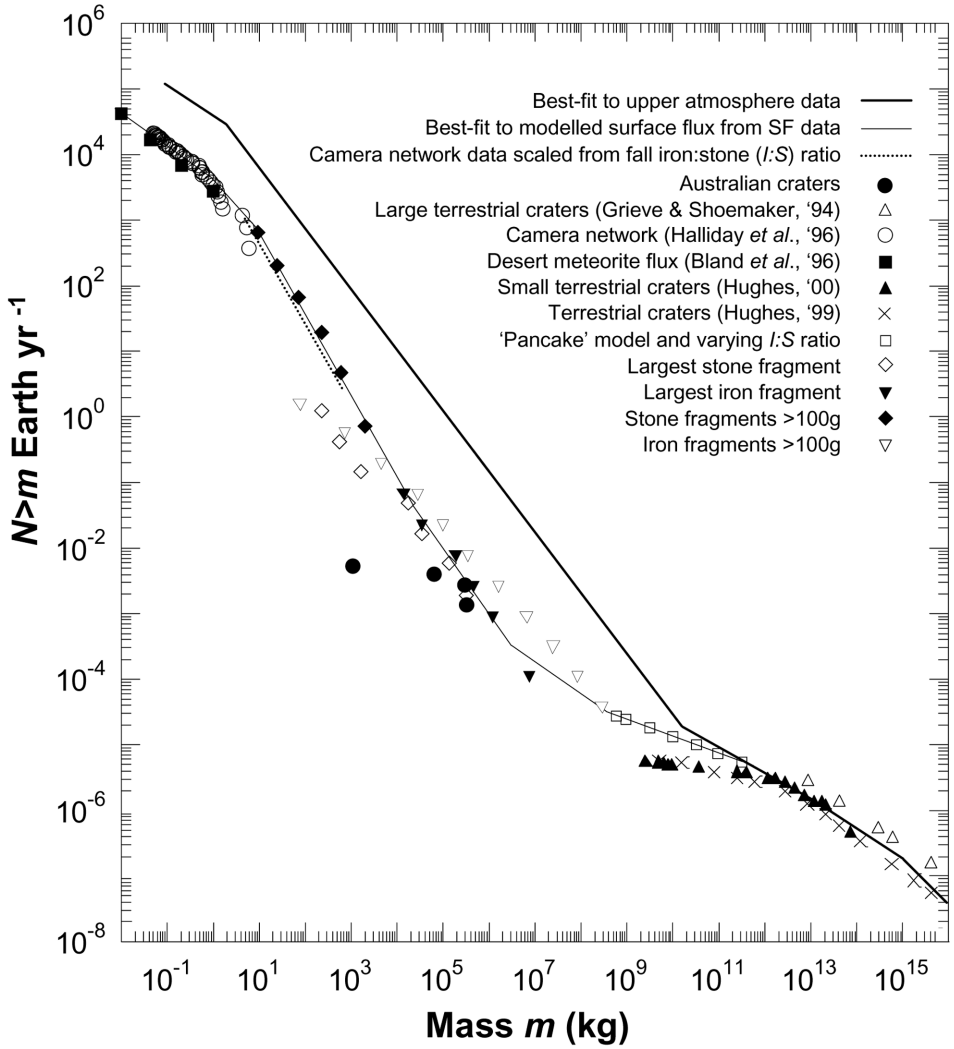

Fig. 16. Estimates of impact rate for the Earth's surface. Our best fit to the upper atmosphere data (see Fig. 15) is shown for reference. The calculated flux at the surface is derived from the best-fit upper atmosphere curve, which is scaled based on the separated fragment and pancake model predictions for mass delivered to the surface for a given pre-entry mass, taking into account variations in the composition of the flux at different masses.

data and relevant data constraining the flux at the surface. The surface flux data are also presented in Table 2, based on scaling from a best-fit to the upper atmosphere data. A comparison with previous flux estimates is shown in Fig. 17.

Converting this data to an approximate interval between impacts of a given size, we anticipate two 10^3 kg events at the Earth's surface every year, a 10^5 kg event every 100 years, a 10^7 kg event every 5,400 years, a 10^9 kg event every 40,000 years, and a 10^{11} kg event every 130,000 years. Converting to cratering rates (for the whole Earth), our analysis predicts an impact of the size of Meteor crater (1.2 km) every 20,000 years, a Wolfe Creek (0.9 km) every 13,000 years, and a Henbury or Odessa (crater fields with largest craters ~0.16 km) every 500 years. We would anticipate a Henbury-sized impact in the British Isles every 1.1 Ma.

Since we chose conservatively high values for stony bolide strength and density, and as it is entirely possible that the proportion of irons at the top of the atmosphere is <5%, our modeled flux curve probably represents an upper limit on surface impact rate for a given flux at the upper atmosphere.

In comparison with previous studies (Fig. 17), our estimate for the flux at the surface of the largest bodies (10^9–10^{11} kg) is substantially lower (there are no data with which to compare for 10^2–10^9 kg bodies). Morrison et al. (1994) and Chapman and Morrison (1994) based their flux estimate on an earlier study by Shoemaker (1983), with 160 m as the cut-off above which stony bodies would crater the surface rather than produce airbursts (Morrison et al. 1994). Their curve predicts a 160 m diameter body arriving at the Earth's surface every ~7,700 years, and a 300 m diameter body every ~31,000 years. These rates are 10× to 4× higher, respectively, than our estimates. They would predict that 7–8 craters >3.8 km should be formed on the Earth's land area every 200 ka. No craters of this size and age are known.

Table 2. Estimates for the impact rate at the Earth's surface, taking our best-fit to the upper atmosphere data set and scaling it based on the results of SF and pancake modeling. As independent estimates for the flux of smaller (0.1–10 kg) meteorites are in agreement (Halliday et al. 1989; Bland et al. 1996), we use that data here. Scaling from mass of impactor to crater size is based on Schmidt and Housen (1987) and assumes 45° impacts, with surface impact velocity varying from 18 km/s for objects >5 × 10^9 kg down to 2 km/s for objects of 25,000 kg, target density of 3000 kg/m^3, and impactor density of 7800 kg/m^3 for irons and 3400 kg/m^3 for stones, with 95% irons forming craters <1.5 km diameter, and 95% stones forming craters >10 km diameter.

Mass (kg)	D_f crater (km)	Frequency ($N >$ m yr^{-1})	Interval ($1/N$)
0.1	N/A	13,710	
0.5	N/A	6217	
1	N/A	4422	
5	N/A	1189	
10	N/A	674	
50	N/A	94	
100	N/A	40	
500	N/A	5.3	
1000	N/A	2.2	
5000	N/A	2.98E – 01	3.4
10,000	N/A	1.00E – 01	10
50,000	0.06	2.01E – 02	50
100,000	0.08	1.01E – 02	99
500,000	0.15	2.03E – 03	492
1,000,000	0.20	1.02E – 03	981
5,000,000	0.36	2.61E – 04	3830
1.00E + 07	0.46	1.86E – 04	5363
5.00E + 07	0.82	8.53E – 05	11,720
1.00E + 08	1.06	6.09E – 05	16,410
5.00E + 08	1.64	2.95E – 05	33,900
1.00E + 09	2.00	2.47E – 05	40,400
5.00E + 09	3.07	1.65E – 05	60,750
1.00E + 10	3.65	1.38E – 05	72,420
5.00E + 10	5.47	9.18E – 06	108,900
1.00E + 11	6.54	7.70E – 06	129,800
5.00E + 11	9.78	5.12E – 06	195,200
1.00E + 12	11.7	3.98E – 06	251,000
5.00E + 12	17.8	2.12E – 06	472,800
1.00E + 13	21.3	1.54E – 06	647,400
5.00E + 13	32.4	7.44E – 07	1,344,000
1.00E + 14	38.8	5.43E – 07	1,840,000
5.00E + 14	58.9	2.62E – 07	3,819,000
1.00E + 15	70.5	1.84E – 07	5,434,000
5.00E + 15	107	6.24E – 08	116,040,000
1.00E + 16	128	3.91E – 08	25,560,000
5.00E + 16	195	1.33E – 08	75,440,000
1.00E + 17	234	8.32E – 09	120,200,000
5.00E + 17	355	2.82E – 09	354,900,000

Ward and Asphaug (2002) also recently considered the impact rate at the Earth's surface, but restricted their study to the relevance of impact rate in quantifying the threat of impact-induced tsunami. Ward (2002) built on this work to consider overall planetary cratering. These studies derived a flux at the top of the atmosphere by assuming a single power law to extrapolate from the small meteoroid light-flash flux data of Nemtchinov et al. (1997) to the large NEO data of Shoemaker et al. (1990) and did not consider curvature in the SFD for upper atmosphere impactors (see Fig. 17). The interaction between bolide and atmosphere was based on earlier pancake model results for stony impactor survival, assuming spreading to 2× initial radius (Toon et al. 1994). Ward (2002) suggest that all bodies >100 m in diameter reach the Earth's surface. The result of this analysis was that Earth should be struck by 100 m bodies every 464 years, by 150 m bodies every 1100 years, and by 200 m bodies every 2500 years (Ward 2002). Taking average asteroidal impact conditions and crater scaling from Schmidt and Housen (1987), this flux would produce 126 craters >2.7 km in diameter on the Earth's land area every 200 ka, 53 of which would be >3.6 km in diameter and 23 of these would be >4.4 km in diameter. No craters of this size and age are known. The largest craters formed in the last 200 ka are Barringer (1.19 km) and Lonar (1.83 km). Our data predict 2–3 craters of 1.2 km or larger formed on the Earth's land area over a 200 ka period.

In terms of the hazard to human populations, our data for the surface flux has specific relevance in quantifying the threat posed by impact-generated tsunami. Ward and Asphaug (2000) have shown that the peak contributors to potentially hazardous tsunami (those >5 m in height) are impactors of ~220 m diameter (an impactor of mass ~2–3 × 10^{10} kg). Their estimate for the frequency of 220 m bolide impacts was 1 every 3000–4000 years (Ward and Asphaug 2000). Our data suggest an impact rate ~26× lower. As Tunguska-like events are unlikely to couple their energy efficiently enough into the ocean surface to generate large tsunami, the implication is that the hazard posed by impact-generated tsunami is lower than previously thought. This analysis is significant in redefining the impact hazard posed by small asteroids.

The Completeness of the Terrestrial Crater Record

Over the 10^{10}–10^{12} kg region, our calculated curve is similar to (although slightly higher than the terrestrial crater data (Hughes 2000). The implication is that severe atmospheric disruption of stony impactors is the primary cause of the departure from the expected SFD for 1.5–10 km craters on Earth, and that the terrestrial crater record on stable, well-explored cratons for the last ~120 Ma is essentially complete for craters larger than 2–3 km, as has been

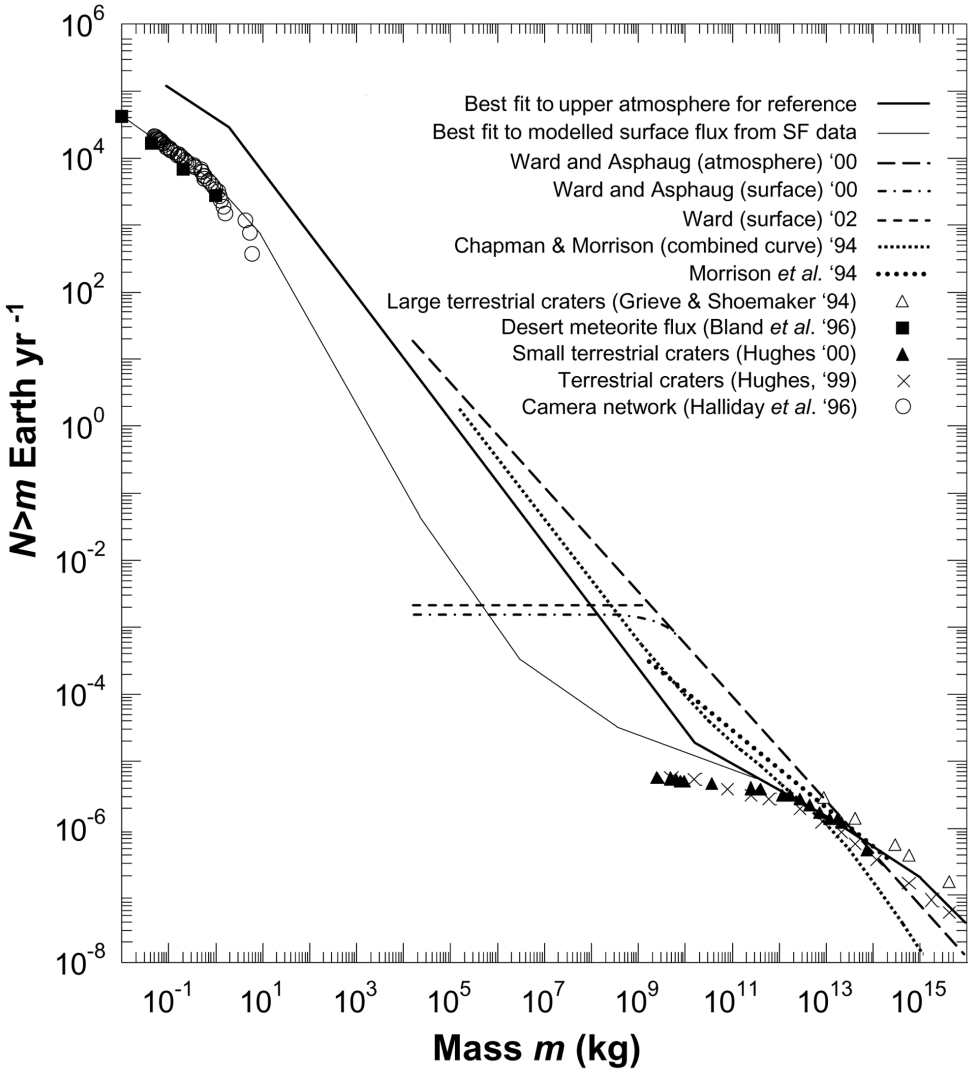

Fig. 17. Earlier impact rate estimates (Chapman and Morrison 1994; Morrison et al. 1994; Ward and Asphaug 2000), compared to our modeled size-frequency distribution of surface impactors. Chapman and Morrison (1994) combine surface and atmosphere flux estimates in a single curve, while Morrison et al. (1994) annotate that curve. Ward and Asphaug (2000) define separate estimates for upper atmosphere and surface.

suggested by Hughes (2000), although with some erosion of the smallest craters.

However, even quite recent small craters are under-represented (with the possible exception of Australia). Our simulations allow us to address the completeness of the terrestrial small crater record, and predict the number of craters of all sizes that we would expect to find in a given area over a given time interval. As an example, we calculate that over the last 50,000 years on the Earth's land area we should expect 90–100 craters >0.1 km (eight have been discovered), 30–35 >0.15 km (five have been discovered), 4–5 >0.3 km (two are known) and 2 >0.5 km (one). Note that this example applies only to the recent crater record—there are many more large craters awaiting discovery that are >50,000 years old in areas that have not been fully explored. Much of South America falls into this category.

Numbers of Large Meteorites in Hot Deserts

The largest meteorites known are Hoba (6×10^4 kg), Cape York (5.8×10^4 kg), and Campo del Cielo (5×10^4 kg). The largest fall is Sikhote-Alin (2.3×10^4 kg recovered). Based on our SF model results for the largest surviving iron fragment over the 10^4–10^5 kg range (i.e., approximately the mass of the largest meteorites), we can estimate that 4–5 iron meteorites in this size range should arrive at the Earth's surface every hundred years. This rate leads to an interesting extrapolation. In Australia, we expect ~10 iron meteorites $>5 \times 10^4$ kg falling in the area of the continent that is effectively desert (35%) every 0.1 Ma. Given known weathering rates (Bland et al. 1998), we would expect meteorites of this size and composition to last much longer than 0.1 Ma in a desert. The recovery of irons such as

Mundrabilla, with very long terrestrial ages, testifies to this. The suggestion is that there should be numbers of extremely large iron meteorites still awaiting discovery in the world's deserts. However, this extrapolation does not take into account survivability of meteorites during the impact. For bodies with pre-atmospheric masses much larger than 10^4–10^5 kg, impact velocity becomes important (Fig. 6)—fragments resulting from the atmospheric disruption of these bodies will create craters, in addition to falling as meteorites (as we know from the Sikhote-Alin fall). Objects with pre-atmospheric masses much larger than 10^5 kg will only form craters (although meteoritic material may survive the crater-forming process e.g., Meteor crater). Our preliminary estimates (Artemieva and Bland 2003) show that very special conditions (low impact velocity, very low impact angle, and oceanic impact site) are needed to keep the largest meteorites intact–the majority of these large chunks are disrupted, melted, and finally create small craters.

CONCLUSIONS

Due to a combination of atmospheric disruption, erosion, infilling, and tectonism, the terrestrial small crater record is incomplete. As a guide to the impact rate at the Earth's surface, it must be used with caution. We have shown that an understanding of the interaction between bolides and the Earth's atmosphere, coupled with a knowledge of the impact rate at the upper atmosphere, is capable of overcoming this problem. Using this approach, we have constructed a complete size frequency distribution for impactors, both at the Earth's surface and the upper atmosphere. Our analysis suggests that:

1. Over the mass range 10^3–10^7 kg iron impactors transfer to the surface ~3 orders of magnitude more energy/unit area than stones, and even large stony bodies of ~10^8–10^{10} kg are inefficient at transferring energy to the surface. Put simply, over this mass range irons dominate the flux at the surface, and stones are disrupted in the atmosphere.
2. Fragmentation is the rule for all impactors less than 1 km. Single craters <10–20 km across may well have been produced by the simultaneous impact of closely spaced fragments rather than a single impactor.
3. Based on a compilation of flux data for top of the Earth's atmosphere, we derive a best fit using a series of power law branches for the upper atmosphere impactor SFD over 16 orders of magnitude.
4. This analysis of the upper atmosphere data set suggests that Tunguska events should happen approximately every 500 years.
5. Taking the curve for the upper atmosphere and scaling it to the Earth's surface based on our modeling results, we find that 100 m craters will be formed on the Earth's land area every 500 years, 0.5 km craters every 21,000 years, and 1 km craters every 52,000 years. This surface impact rate is consistent with meteorite flux data from camera network and desert studies, and for larger meteorite masses, with an extension of the camera network data set based on the observed depletion in stony meteorites at higher masses. In the ~10^5 kg range, it is also consistent with the production of small recent craters in Australia—a time period and location that should allow preservation of even small impact features.
6. Our surface flux curve is broadly consistent with, although slightly higher than, the SFD for 2–10 km craters on Earth, suggesting that atmospheric disruption is the primary cause of the departure from the expected asteroidal SFD for craters <10 km, but also that erosion becomes increasingly important for smaller craters.
7. Bodies capable of producing hazardous tsunami (~200 m in diameter projectiles) should strike the Earth every ~100,000 years.
8. Although the largest iron meteorites (e.g., Hoba) will typically arrive at velocities that cause cratering, smaller iron fragments should decelerate to survivable velocities. The flux of these smaller 10^3–10^4 kg objects indicates that there may be many more large iron meteorites awaiting discovery in desert regions.

Acknowledgments–N. A. thanks RFBR for financial support, and P. A. B. thanks the Royal Society for their support. The authors would also like to thank Boris Ivanov, Bill Hartmann, and Peter Brown for providing cratering data, flux data, and valuable discussion; John Stephenson for assistance in fitting various datasets; and H. Jay Melosh, Ian Halliday, Bill Bottke, Clarke Chapman, Valerie Shuvalov, Jo Morgan, Betty Pierazzo, and Matthieu Gounelle for valuable suggestions and advice. This paper also benefited from constructive reviews by Boris Ivanov and David Hughes. This paper is IARC publication number 2005-0728.

Editorial Handling—Dr. Wolf Uwe Reimold

REFERENCES

Artemieva N. A. and Bland P. A. 2003. Crater fields on Venus, Earth, and Mars (abstract #1319). 34th Lunar and Planetary Science Conference. CD-ROM.

Artemieva N. A. and Shuvalov V. V. 1996. Interaction of shock waves during the passage of a disrupted meteoroid through the atmosphere. *Shock Waves* 5:359–367.

Artemieva N. A. and Shuvalov V. V. 2001. Motion of a fragmented meteoroid through the planetary atmosphere. *Journal of Geophysical Research* 106:3297–3310.

Bailey M. E. and Stagg C. R. 1988. Cratering constraints on the inner Oort Cloud: Steady-state models. *Monthly Notices of the Royal Astronomical Society* 235:1–35.

Bailey M. E. and Emel'yanekno V. V. 1998. Cometary capture and the nature of the impactors. In *Meteorites: Flux with time and impact effects,* edited by Grady M. M., Hutchison R., McCall G. J. H., and Rothery D. A. London: Geological Society, Special Publication 140. pp. 11–17.

Binzel R. P., Harris A. W., Bus S. J., and Burbine T. H. 2001. Spectral

properties of near-Earth objects: Palomar and IRTF results for 48 objects including spacecraft targets (9969) Braille (10302) and 1989 ML. *Icarus* 151:139–149.

Binzel R. P., Lupishko D. F., Di Martino M., Whiteley R. J, and Hahn G. J. 2003. Physical properties of near-Earth objects. In *Asteroids III,* edited by Bottke W. F., Cellino A., Paolicchi P., and Binzel R. P. Tucson, Arizona: The University of Arizona Press. pp. 255–271.

Bland P. A., Sexton A., Jull A. J. T., Berry F. J., Bevan A. W. R., Thornley D., Astin T., and Pillinger C. T. 1998. Climate and rock weathering: A study of terrestrial age dated ordinary chondritic meteorites from hot desert regions. *Geochimica et Cosmochimica Acta* 62:3169–3184.

Bland P. A., Smith T. B., Jull A. J. T., Berry F. J., Bevan A. W. R., Cloudt S., and Pillinger C. T. 1996. The flux of meteorites to the Earth over the last 50,000 years. *Monthly Notices of the Royal Astronomical Society* 283:551–565.

Bland P. A. and Artemieva N. A. 2003. Efficient disruption of small asteroids by Earth's atmosphere. *Nature* 424:288–291.

Bottke W. F., Jr., Durda D. D., Nesvorný D., Jedicke R., Morbidelli A., Vokrouhlický D., and Levison H. 2005. The fossilized size distribution of the main asteroid belt. *Icarus* 175:111–140.

Bottke W. F., Jr., Nesvorný D., and Durda D. D. 2005. Are most small craters primaries or secondaries: Insights from asteroid collisional/dynamical evolution models (abstract #1489). 36th Lunar and Planetary Science Conference. CD-ROM.

Brown P., Spalding R. E., ReVelle D. O., Tagliaferri E., and Worden S. P. 2002. The flux of small near-Earth objects colliding with the Earth. *Nature* 420:294–296.

Burbine T. H. 2002. Asteroids: Their composition and impact threat. *Bulletin of the Czech Geological Survey* 77:71–80.

Bus S. J. and Binzel R. P. 2002. Phase II of the small main belt asteroid spectroscopic survey: A feature-based taxonomy. *Icarus* 158: 146–177.

Ceplecha Z. and ReVelle D. O. 2005. Fragmentation model of meteoroid motion, mass loss, and radiation in the atmosphere. *Meteoritics & Planetary Science* 40:35–54.

Ceplecha Z., Spurný P., Borovička J., and Keclíková J. 1993. Atmospheric fragmentation of meteoroids. *Astronomy & Astrophysics* 279:615–626.

Chapman C. R. and Morrison D. 1994. Impacts on the Earth by asteroids and comets: Assessing the hazard. *Nature* 367:33–39.

Chyba C. F., Thomas P. J., and Zahnle K. J. 1993. The 1908 Tunguska explosion: Atmospheric disruption of a stony asteroid. *Nature* 361:40–44.

Cochrane C. 2002. Depth/diameter ratios of impact craters on Venus (abstract #MS014). Proceedings, 36th Vernadsky Institute/Brown University Microsymposium in Comparative Planetology.

Consomagno G. J., Britt D. T., and Stoll C. P. 1998. The porosity of ordinary chondrites: Models and interpretations. *Meteoritics & Planetary Science* 33:1221–1229.

Crawford D. A. 1997. Comet Shoemaker-Levy 9 fragment size estimates: How big was the parent body? *Annals of the New York Academy of Sciences: Near-Earth Objects.* 822:155–173.

Dohnanyi J. W. 1969. Collisional models of asteroids and their debris. *Journal of Geophysical Research* 74:2531–2554.

Earth Impact Database, http://www.unb.ca/passc/ImpactDatabase. Last accessed November 10, 2005.

Farinella P., Paolicchi P., and Zappala V. 1982. Fragmentation of Hyperion and cratering of Saturn's satellites. *Hvar Observatory Bulletin* 6:167.

Farinella P., Milani A., Nobili A. M., Paolicchi P., and Zappala V. 1983. Hyperion—Collisional disruption of a resonant satellite. *Icarus* 54:353–360.

Fujiwara A. and Tsukamoto A. 1980. Experimental study on the velocity of fragments in collisional breakup. *Icarus* 44:142–153.

Gault D. E., Hörz F., and Hartung J. B. 1972. Effects of microcratering on the lunar surface. Proceedings, 3rd Lunar Science Conference. p. 2713–2734.

Gilbert G. K. 1893. The Moon's face, a study of the origin of its features. *Bulletin of the Philosopical Society of Washington* 12: 241–292.

Grady D. E. and Lipkin J. 1980. Criteria for impulsive rock fracture. *Geophysical Research Letters* 7:255–258.

Grady M. M. 2000. *Catalogue of meteorites*, 5th ed. Cambridge: Cambridge University Press.

Grieve R. A. F. and Shoemaker E. M. 1994. The record of past impacts on Earth. In *Hazards due to comets and asteroids,* edited by Gehrels T. Tucson, Arizona: The University of Arizona Press. pp. 417–462.

Gurov E. P. 1996. The group of Macha Craters in Western Yakutia (abstract). 27th Lunar and Planetary Science Conference. p. 473.

Halliday I., Blackwell A. T., and Griffin A. A. 1989. The flux of meteorites on the Earth's surface. *Meteoritics* 24:173–178.

Halliday I., Griffin A. A., and Blackwell A. T. 1996. Detailed data for 259 fireballs from the Canadian camera network and inferences concerning the influx of large meteoroids. *Meteoritics & Planetary Science* 31:185–217.

Harris A. W. 2003. Just how many Tunguskas are there? Recent progress in estimating the size-frequency distribution of NEAs. Proceedings, Asteroids, Comets, Meteors 2002.

Hartmann W. K. 1967. Lunar crater counts II: Three lunar-surface-type areas. *Communications of the Lunar and Planetary Laboratory* 7:145–156.

Hartmann W. K. 1970. Preliminary note on lunar cratering rates and absolute time scales. *Icarus* 12:131–133.

Hartmann W. K. 1977. Relative crater production rates on planets. *Icarus* 31:260–276.

Hartmann W. K. 1999. Martian crater counting VI: Crater count isochrons and evidence for recent volcanism from Mars Global Surveyor. *Meteoritics & Planetary Science* 34:167–177.

Hartmann W. K. and Neukum G. 2001. Cratering chronology and the evolution of Mars. *Space Science Reviews* 96:165–194.

Hartmann W. K., Strom R. G., Grieve R. A. F., Weidenschilling S. J., Diaz J., Blasius K. R., Chapman C. R., Woronow A., Shoemaker E. M., Dence M. R., and Jones K. L. 1981. Chronology of planetary volcanism by comparative studies of planetary cratering. In *Basaltic volcanism on the terrestrial planets, Basaltic Volcanism Study Project.* New York: Pergamon Press. pp. 1050–1129.

Hiesinger H., Head J. W., Wolf U., Jaumann R., and Neukum G. 2003. Ages and stratigraphy of mare basalts in Oceanus Procellarum, Mare Nubium, Mare Cognitum, and Mare Insularum. *Journal of Geophysical Research*, doi:10.1029/2002JE001985.

Herrick R. R. and Lyons S. N. 1998. Inversion of crater morphometric data to gain insight onto the cratering process. *Meteoritics & Planetary Science* 33:131–143.

Hills J. G. and Goda M. P. 1993. The fragmentation of small asteroids in the atmosphere. *The Astronomical Journal* 105:1114–1144.

Hills J. G. and Goda M. P. 1998. Damage from the impacts of small asteroids. *Planetary and Space Science* 46:219–229.

Hughes D. W. 1994. Comets and asteroids. *Contemporary Physics* 35: 75–93.

Hughes D. W. 2000. A new approach to the calculation of the cratering rate of the Earth over the last 125 ± 20 Myr. *Monthly Notices of the Royal Astronomical Society* 317:429–437.

Ivanov B. A., Basilevsky A. T., and Neukum G. 1997. Atmospheric entry of large meteoroids: Implication to Titan. *Planetary and Space Science* 45:993–1007.

Ivanov B. A., Neukum G., and Wagner R. 2001. Size-frequency distributions of planetary impact craters and asteroids. In *Collisional processes in the solar system,* edited by Marov M. Y.

and Rickman H. Dordrecht: Kluwer Academic Publishers. pp. 1–34.

Ivanov B. A., Neukum G., Bottke W. F., and Hartmann W. K. 2003. The comparison of size-frequency distributions of impact craters and asteroids and the planetary cratering rate. In *Asteroids III,* edited by Bottke W. F., Cellino A., Paolicchi P., and Binzel R. P. Tucson, Arizona: The University of Arizona Press. pp. 89–101.

Ivanov B. A. 2001. Mars/Moon cratering ratio estimates. In *Chronology and evolution of Mars,* edited by Kallenbach R., Geiss J., and Hartmann W. K. Dordrecht: Kluwer Academic Publishers. pp. 87–104.

Koeberl C. 1998. Identification of meteoritic components in impactites. In *Meteorites: Flux with time and impact effects,* edited by Grady M. M., Hutchison R., McCall G. J. H., and Rothery D. A. London: Geological Society. pp. 133–153.

Kyte F. T. 1998. A meteorite from the Cretaceous/Tertiary boundary. *Nature* 396:237–239.

Levison H. F., Morbidelli A., Dones L., Jedicke R., Wiegert P. A., and Bottke W. F. 2002. The mass disruption of Oort Cloud comets. *Science* 296:2212–2215.

McDonald I. 2002. Clearwater East impact structure: A reinterpretation of the projectile type using new platinum-group element data from meteorites. *Meteoritics & Planetary Science* 37:459–464.

McDonald I., Andreoli M. A. G., Hart R. J., and Tredoux M. 2001. Platinum-group elements in the Morokweng impact structure, South Africa: Evidence for the impact of a large ordinary chondrite projectile at the Jurassic-Cretaceous boundary. *Geochimica et Cosmochimica Acta* 65:299–309.

McEwen A., Preblich B., Turtle E., Studer D., Artemieva N., Golombek M., Hurst M., Kirk R., and Burr D. 2005. Distant secondary craters and age constraints on young Martian terrains (abstract #2111). 36th Lunar and Planetary Science Conference. CD-ROM.

McKinnon W. B., Zahnle K. J., Ivanov B. A., and Melosh H. J. 1997. Cratering on Venus: Models and observations. *In Venus II: Geology, geophysics, atmosphere, and solar wind environment,* edited by Bougher S. W., Hunten D. M., and Philips R. J. Tucson, Arizona: The University of Arizona Press. 969 p.

Melosh H. J. 1981. Atmospheric breakup of terrestrial impactors. In *Multi-ring basins,* edited by Schultz P. H. and Merrill R. B. New York: Pergamon Press. pp 29–35.

Melosh H. J. 1989. *Impact cratering: A geological process.* Oxford: Oxford University Press. 245 p.

Melosh H. J. and Collins G. S. 2005. Meteor crater formed by low-velocity impact. *Nature* 434:157.

Milton D. J. 1972. Structural geology of the Henbury meteorite craters, Northern Territory, Australia. U.S. Geological Survey Professional Paper #599-C. pp. C1–C17.

Moore H. J., Plaut J. J., and Parker T. J. 1993. Relief of some small landforms on Venus (abstract). 24th Lunar and Planetary Science Conference. pp. 1003–1004.

Morbidelli A., Jedicke R., Bottke W. F., Michel P., and Tedesco E. F. 2002. From magnitudes to diameters: The albedo distribution of near-Earth objects and the Earth collision hazard. *Icarus* 158:329–343.

Morrison D., Chapman C. R., and Slovic P. 1994. The impact hazard. In *Hazards due to comets and asteroids,* edited by Gehrels T. Tucson, Arizona: The University of Arizona Press. pp 59–91.

Napier W. M. 1998. Galactic periodicity and the geological record. In *Meteorites: Flux with time and impact effects,* edited by Grady M. M., Hutchison R., McCall G. J. H., and Rothery D. A. London: Geological Society. pp. 19–29.

Napier W. M. and Clube S. V. M. 1979. A theory of terrestrial catastrophism. *Nature* 282:455–459.

Nemtchinov I. V., Svetsov V. V., Kosarev I. B., Golub' A. P., Popova O. P., and Shuvalov V. V. 1997. Assessment of the kinetic energy of meteoroids detected by satellite-based light sensors. *Icarus* 130:259–274.

Neukum G. and Wise D. U. 1976. Mars: A standard crater curve and possible new timescale. *Science* 194:1381–1387.

Neukum G. and Ivanov B. A. 1994. Crater size distributions and impact probabilities on Earth from lunar, terrestrial-planet, and asteroid cratering data. In *Hazards due to comets and asteroids,* edited by Gehrels T. Tucson, Arizona: The University of Arizona Press. pp. 359–416.

Neukum G., König B., Fechtig H., and Storzer D. 1975. Cratering in the Earth-Moon system: Consequences for age determination by crater counting. Proceedings, 6th Lunar Science Conference. pp. 2597–2620.

Neukum G., Ivanov B. A., and Hartmann W. K. 2001. Cratering records in the inner solar system in relation to the lunar reference system. In *Chronology and evolution of Mars,* edited by Kallenbach R., Geiss J., and Hartmann W. K. Dordrecht: Kluwer Academic Publishers. pp. 55–86.

O'Keefe J. D., Takata T., and Ahrens T. J. 1994. Penetration of large bolides into dense planetary atmospheres—Role of instabilities (abstract). 25th Lunar and Planetary Science Conference. pp.1023–1024.

Passey Q. R. and Melosh H. J. 1980. Effects of atmospheric breakup on crater field formation. *Icarus* 42:211–233.

Plescia J. B. 2005. Small-diameter Martian craters: Applicability for chronology—or not (abstract #2171). 36th Lunar and Planetary Science Conference. CD-ROM.

Rabinowitz D. 1993. The size-distribution of the Earth-approaching asteroids. *The Astrophysical Journal* 407:412–427.

Rabinowitz D., Helin E., Lawrence K., and Pravdo S. 2000. A reduced estimate of the number of kilometre-sized near-Earth asteroids. *Nature* 403:165–166.

Rajan R. S. and ReVelle D. O. 1988. Identification of nickel-iron material among the Prairie Network fireballs. *Bulletin of the American Astronomical Society* 20:862.

Rampino M. R. and Haggerty B. M. 1994. Extraterrestrial impacts and mass extinctions of life. In *Hazards due to comets and asteroids,* edited by Gehrels T. Tucson, Arizona: The University of Arizona Press. pp. 827–857.

Rampino M. R. and Stothers R. B. 1984. Terrestrial mass extinctions, cometary impacts, and the Sun's motion perpendicular to the galactic plane. *Nature* 308:709–712.

Raup D. M. and Sepkoski J. J. 1984. Periodicity of extinctions in the geological past. *Proceedings of the National Academy of Sciences* 81:801–805.

ReVelle D. O. 1997. Historical detection of atmospheric impacts by large bolides using acoustic-gravity waves. *Annals of the New York Academy of Science* 822:284–302.

ReVelle D. O. and Ceplecha Z. 1994. Analysis of identified iron meteoroids: Possible relation with M-type Earth-crossing asteroids? *Astronomy and Astrophysics* 292:330–336.

Schmidt R. M. and Housen K. R. 1987. Some recent advances in the scaling of impact and explosion cratering. *International Journal of Impact Engineering* 5:543–560.

Schultz P. H. and Gault D. E. 1985. Clustered impacts: Experiments and implications. *Journal of Geophysical Research* 90:3701–3732.

Shoemaker E. M. 1962. Interpretation of lunar craters. In *Physics and Astronomy of the Moon,* edited by Kopal Z. San Diego: Academic Press. pp. 283–359.

Shoemaker E. M. 1965. Preliminary analysis of the fine structure of the lunar surface in Mare Cognitum. JPL-NASA Technical Report #32-700. 75 p.

Shoemaker E. M. 1977. Astronomically observable crater-forming

projectiles. In *Impact and explosion cratering,* edited by Roddy D. J., Pepin R. O., and Merrill R. B. New York: Pergamon Press. pp. 617–628.

Shoemaker E. M. 1983. Asteroid and comet bombardment of the Earth. *Annual Reviews of Earth and Planetary Science* 11:461–494.

Shoemaker E. M. 1998. Long-term variations in the impact cratering rate on Earth. In *Meteorites: Flux with time and impact effects,* edited by Grady M. M., Hutchison R., McCall G. J. H., and Rothery D. A. London: Geological Society. pp. 7–10.

Shoemaker E. M. and Shoemaker C. S. 1988. Impact structure of Australia (1987) (abstract). 19th Lunar and Planetary Science Conference. p. 1079.

Shoemaker E. M. and Shoemaker C. S. 1990. Proterozoic impact record of Australia. In *International Workshop on Meteorite Impact on the Early Earth.* Houston: Lunar and Planetary Institute. LPI Contribution #746. pp. 47–48.

Shoemaker E. M., Wolfe R. F., and Shoemaker E. M. 1990. Asteroid and comet flux in the neighborhood of the Earth. In *Global catastrophes in Earth history: An interdisciplinary conference on impacts, volcanism, and mass mortality,* edited by Sharpton V. L. and Ward P. D. GSA Special Paper #247. Boulder, Colorado: Geological Society of America. pp. 155–170.

Shukolyukov A. and Lugmair G. W. 1998. Isotopic evidence for the Cretaceous-Tertiary impactor and its type. *Science* 282:927–929.

Shukolyukov A. and Lugmair G. W. 2000. Extraterrestrial matter on Earth: Evidence from the Cr isotopes. In *Catastrophic events and mass extinctions: Impacts and beyond.* LPI Contribution #1053. Houston: Lunar and Planetary Institute. pp. 197–198.

Shukolyukov A., Lugmair G. W., Koeberl C., and Reimold W. U. 1999. Chromium in the Morokweng impact melt: Isotopic evidence for extraterrestrial component and type of the impactor (abstract). *Meteoritics & Planetary Science* 34:A107–A108.

Shukolyukov A., Kyte F. T., Lugmair G. W., Lowe D. R., and Byerly G. R. 2000. The oldest impact deposits on Earth—First confirmation of an extraterrestrial component. In *Impacts and the early Earth,* edited by Gilmour I. and Koeberl C. Berlin: Springer-Verlag. pp. 99–115.

Shuvalov V. V., Artemieva N. A., and Trubetskaya I. A. 2000. Simulating the motion of a disrupted meteoroid with allowance for evaporation. *Solar System Research* 34:49–60.

Shuvalov V. V. and Artemieva N. A. 2002. Numerical modeling of Tunguska-like impacts. *Planetary and Space Science* 50:181–192.

Schmidt R. M. and Housen K. R. 1987. Some recent advances in the scaling of impact and explosion cratering. *International Journal of Impact Engineering* 5:543–560.

Stuart J. S. 2001. A near-Earth asteroid population estimate from the LINEAR survey. *Science* 294:1691–1693.

Svetsov V. V., Nemtchinov I. V., and Teterev A. V. 1995. Disintegration of large meteoroids in Earth's atmosphere: Theoretical models. *Icarus* 116:131–153.

Toon O. B., Zahnle K., Turco R. P., and Covery C. 1994. Environmental perturbations caused by asteroid impacts. In *Hazards due to comets and asteroids,* edited by Gehrels T. Tucson, Arizona: The University of Arizona Press. pp 791–826.

Tsvetskov V. I. and Skripnik A. Ya. 1991. Atmospheric fragmentation of meteorites according to strength theory. *Solar System Research* 25:273–279.

Ward S. N. 2002. Planetary cratering: A probabilistic approach. *Journal of Geophysical Research* 107:7-1–7-11.

Ward S. N. and Asphaug E. 2000. Asteroid impact tsunami: A probabilistic hazard assessment. *Icarus* 145:64–78.

Weissman P. R. 1990. The cometary impactor flux at the Earth. In *Global catastrophes in Earth history: An interdisciplinary conference on impacts, volcanism, and mass mortality,* edited by Sharpton V. L. and Ward P. D. Special Paper #247. Boulder, Colorado: Geological Society of America. pp. 171–180.

Werner S. C., Harris A. W., Neukum G., and Ivanov B. A. 2002. The near-Earth asteroid size-frequency distribution: A snapshot of the lunar impactor size-frequency distribution. *Icarus* 156:287–290.

Zahnle K., Schenk P., Levinson H., and Dones L. 2003. Cratering rates in the outer solar system. *Icarus* 163:263–289.

Zotkin I. T. and Tsvetkov V. I. 1983. On the form of iron meteorites. *Solar System Research* 17:60–62.